Many-body quantum interference route to the two-channel Kondo effect: Inverse design for molecular junctions

Sudeshna Sen[1] and Andrew K. Mitchell[2, 3, *]

[1]*Department of Physics, IIT(ISM) Dhanbad, Dhanbad-826004, Jharkhand, India*
[2]*School of Physics, University College Dublin, Belfield, Dublin 4, Ireland*
[3]*Centre for Quantum Engineering, Science, and Technology, University College Dublin, Ireland*

Molecular junctions – whether actual single molecules in nanowire break junctions or artificial molecules realized in coupled quantum dot devices – offer unique functionality due to their orbital complexity, strong electron interactions, gate control, and many-body effects from hybridization with the external electronic circuit. Inverse design involves finding candidate structures that perform a desired function optimally. Here we develop an inverse design strategy for generalized quantum impurity models describing molecular junctions, and as an example, use it to demonstrate that many-body quantum interference can be leveraged to realize the two-channel Kondo critical point in simple 4- or 5-site molecular moieties. We show that remarkably high Kondo temperatures can be achieved, meaning that entropy and transport signatures should be experimentally accessible.

Nanoelectronics circuits are quantum devices featuring a nanostructure with a few confined and typically strongly correlated degrees of freedom coupled to source and drain metallic leads [1–5]. For molecular junctions, a single molecule can bridge the gap in a nanowire [6]. The electrical conductance of such a junction is controlled by the structure and chemistry of the molecule, through which a current must pass [7]. A range of physics can be realized in such systems – including Coulomb blockade and various Kondo effects [4, 8–11], quantum interference [12–17], and phase transitions [18, 19]. This presents the tantalizing possibility of devices at the limit of miniaturization that leverage inherently quantum effects to provide enhanced functionality as switches [20–23], transistors [4, 5], diodes and rectifiers [24–29], and even as tools for chemical analysis [30]. A grand challenge in the field is to find molecular species that can form robust junctions to perform a desired function optimally [31].

Simple artificial molecular junctions can also be fabricated in semiconductor coupled quantum dot (QD) devices [32, 33]. The design of such systems need not obey chemical structure principles [34], and they benefit from *in-situ* tunability [35]. They can also be integrated with other components to realize more exotic effects, such as fractionalization at the two-channel Kondo (2CK) quantum critical point [36], which results from the frustration of screening when a single spin-$\frac{1}{2}$ degree of freedom is coupled to two independent conduction electron channels [37]. The 2CK effect has gained prominence recently as a route to engineer many-body Majorana zero modes in nanostructures [38–41]. Spectacular experimental realizations of 2CK physics in QD systems [42–44] have however required the use of a 'quantum box' or metallic island to provide a reservoir of many interacting electrons [45, 46]. Can the 2CK effect be realized in simpler QD systems without the use of these components? If so, what is the minimum number of interacting sites needed? Can we find molecular moieties that realize 2CK physics when placed in a junction?

Model.– Molecular junctions and QDs are described by generalized quantum impurity models [47] of the form $\hat{H} = \hat{H}_{\text{mol}} + \hat{H}_{\text{leads}} + \hat{H}_{\text{hyb}} + \hat{H}_{\text{gate}}$. Here we formulate the isolated molecule as an extended Hubbard Hamiltonian,

$$\hat{H}_{\text{mol}} = \sum_{\sigma=\uparrow,\downarrow} \sum_{m,n} t_{mn} d^{\dagger}_{m\sigma} d_{n\sigma} + \tfrac{1}{2} \sum_{m,n} U_{mn} \hat{n}_m \hat{n}_n \quad (1)$$

where $d^{(\dagger)}_{m\sigma}$ annihilates (creates) an electron on molecule orbital m with spin σ and $\hat{n}_m = \sum_\sigma d^{\dagger}_{m\sigma} d_{m\sigma}$ is a number operator. Single-particle processes are parameterized by t_{mn} whereas U_{mn} embodies electronic interactions. The gate voltage V_g controls the charge on the molecule via $\hat{H}_{\text{gate}} = V_g \sum_m \hat{n}_m$. The leads are described by continua of free fermions, $\hat{H}_{\text{leads}} = \sum_{\alpha,\sigma} \epsilon_k c^{\dagger}_{\alpha\sigma k} c_{\alpha\sigma k}$ with $\alpha = s, d$ for source and drain. The molecule frontier orbital $d_{r_\alpha \sigma}$ couples to a local orbital $c_{\alpha\sigma}$ of lead α via $\hat{H}_{\text{hyb}} = \sum_{\alpha,\sigma} V_\alpha (d^{\dagger}_{r_\alpha \sigma} c_{\alpha\sigma} + \text{H.c.})$, where $c_{\alpha\sigma} = \frac{1}{V_\alpha} \sum_k V_k c_{\alpha\sigma k}$.

Strong electron interactions[3, 4] produce rich many-body physics but also preclude brute force solutions [47]. Inverse design is challenging because physical properties then depend in a highly nontrivial way on the delicate interplay of many microscopic parameters. It is a formidable task to find a set of model parameters that yield specific device functionalities. However, if only the *low-temperature* behavior is of interest, then simpler low-energy effective models may be used [48, 49]. The connection between effective model parameters and low-temperature physical properties is more transparent.

Here we focus on one such scenario, where the low-temperature physics that we seek is that of the 2CK critical point [50]. The condition for obtaining this behavior in molecular junctions is simply stated in terms of the low-energy effective 2CK model. Inverse design then consists of finding the set of microscopic model parameters satisfying this condition. We show that this is achievable in remarkably simple systems, with just a few interacting degrees of freedom, and without the interacting electron reservoirs used previously in experiments [42–44].
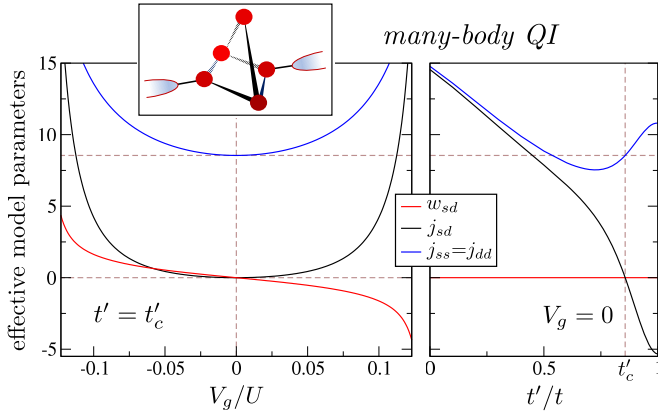
FIG. 1. The simplest molecular moiety to exhibit the 2CK effect with 5 interacting active orbitals. The effective molecule-lead Kondo interactions j_{ss} and j_{dd} are equal and antiferromagnetic (blue line), while source-drain mixing terms vanish due to many-body QI. Potential scattering w_{sd} (red) vanishes at gate voltage $V_g = 0$ by particle-hole symmetry, whereas exchange cotunneling j_{sd} (black) vanishes on tuning the couplings t'/t. Obtained here via SWT and plotted for $U/t = 1$.

Effective models.– An odd number of electrons can be accommodated on the molecule by tuning gate voltages, such that the ground state of $\hat{H}_{\rm mol}$ is a unique spin-doublet state. At low temperatures, effective spin-flip Kondo exchange interactions and potential scattering are generated, described by a generalized 2CK model [51],

$$\hat{H}_{\rm eff} = \hat{H}_{\rm leads} + \sum_{\alpha,\beta} \left[J_{\alpha\beta}\, \hat{\vec{\mathbb{S}}} \cdot \hat{\vec{s}}_{\alpha\beta} + W_{\alpha\beta} \sum_{\sigma} c^{\dagger}_{\beta\sigma} c_{\alpha\sigma} \right] \quad (2)$$

where $\hat{\vec{\mathbb{S}}}$ is a spin-$\frac{1}{2}$ operator for the molecule ground state doublet and $\hat{\vec{s}}_{\alpha\beta} = \frac{1}{2} \sum_{ss'} c^{\dagger}_{\beta s'} \vec{\sigma}_{s's} c_{\alpha s}$ are conduction electron spin operators. We refer to the $J_{\alpha\beta}$ and $W_{\alpha\beta}$ terms as exchange and potential scattering, respectively. The form of Eq. 2 is guaranteed by $SU(2)$ spin symmetry if only the most RG relevant terms are considered [17]. Since $J_{sd} = J_{ds}$ and $W_{sd} = W_{ds}$ by hermiticity, the low-energy behavior of such molecular junctions is controlled by just six effective parameters.

The 2CK critical point arises for equal antiferromagnetic Kondo interactions $J_{ss} = J_{dd} > 0$, but when the source-drain mixing terms vanish, $J_{sd} = W_{sd} = 0$ [50, 52]. In molecular junctions or coupled QD devices, the 2CK effect should be realizable when the molecule or QD has a net spin-$\frac{1}{2}$ ground state and when the effective model parameters satisfy these conditions. W_{ss} and W_{dd} are RG irrelevant and play no role in the following.

Quantum interference (QI) and conductance nodes.– Single-molecule junctions often exhibit QI phenomena, with the most dramatic effect being electrical conductance nodes due to the destructive interference of competing transport pathways through the molecule [13–16]. However, such a description of the QI and transport is

typically on the single-particle level encoded by the real-space hopping matrix t_{nm} [53], and is inapplicable for interacting systems displaying Coulomb blockade or Kondo effects. Many-body QI [17, 54] is naturally richer since it applies in Fock space, which has a much higher complexity, and provides new channels for QI (e.g. between particles and holes). On the level of the effective 2CK model Eq. 2, many-body QI can cause any of the parameters $J_{\alpha\beta}$ and $W_{\alpha\beta}$ to vanish. $J_{sd} = W_{sd} = 0$ must produce a conductance node because then the charge in the leads is separately conserved. The 2CK critical point therefore arises at a conductance node, which can be driven by many-body QI. We dub this the QI-2CK effect.

Perturbative solution.– We consider first the perturbative derivation of the effective 2CK parameters from those of the bare model by means of a generalized Schrieffer-Wolff transformation (SWT) [48]. This is done by projecting the full model for the junction onto the spin-doublet molecule ground states by eliminating virtual excitations to second order in $\hat{H}_{\rm hyb}$. In the Supplementary Information (SI) [51] we formulate this problem in an efficient way that does not require full diagonalization of $\hat{H}_{\rm mol}$, but only uses information on the ground state energy and wavefunction of the isolated molecule. Comparatively large systems can then be treated by using methods that target ground state properties [55–57].

Eq. 2 is obtained by SWT with effective parameters $J_{\alpha\beta} \equiv V_{\alpha}V_{\beta}j_{\alpha\beta}$ and $W_{\alpha\beta} \equiv V_{\alpha}V_{\beta}w_{\alpha\beta}$ that can be calculated from many-body scattering amplitudes $A^{\sigma\alpha\beta} = p^{\sigma\alpha\beta} - h^{\sigma\alpha\beta}$ which involve the tunneling of both particles (p) and holes (h) with spin-σ through the molecule from lead α to lead β. We may write $j_{\alpha\beta} = 2(A^{\uparrow\alpha\beta} - A^{\downarrow\alpha\beta})$ and $w_{\alpha\beta} = \frac{1}{2}(A^{\uparrow\alpha\beta} + A^{\downarrow\alpha\beta})$, with the p and h amplitudes obtainable in closed form as detailed in the SI [51].

Many body QI can appear here in different ways: through the vanishing of individual p or h processes due to interference of competing Fock space propagators, by a cancellation of terms with different spin, or by a cancellation of p and h amplitudes for a given process.

In fact, particle-hole (ph) symmetry guarantees the latter, since then $p^{\sigma\alpha\beta} = h^{-\sigma\alpha\beta}$ and hence $W_{ss} = W_{dd} = W_{sd} = 0$ in Eq. 2. A system is ph-symmetric when its Hamiltonian is invariant to the ph transformations $d_{n\sigma} \to e^{i\phi_{n\sigma}} d^{\dagger}_{n\sigma}$ for all $n\sigma$ (with suitable phases $\phi_{n\sigma}$). The celebrated Coulson-Rushbrooke pairing theorem [58] is a statement about ph symmetry, with p and h excitations appearing symmetrically around the ground state for molecules satisfying the 'starring rule' [54, 59]. A system may exhibit ph symmetry if the molecular structure encoded by the single-particle adjacency matrix t_{mn} can be accommodated on a bipartite graph. Therefore ph-symmetric systems must *not* have odd loops.

Satisfying the 2CK condition.– Since ph symmetry implies $W_{sd} = 0$, we search for ph-symmetric systems in which $J_{sd} = 0$ can also be achieved. In addition we want $J_{ss} = J_{dd}$ for the 2CK effect so we consider only sd-

symmetric molecular moieties. As a simple starting point we study M-site Hubbard chains with constant nearest neighbour hopping t, local Coulomb repulsion U, and local potential $\epsilon = -U/2$. Leads s and d are connected to molecule sites 1 and M. For odd M the ground state around $V_g = 0$ is a unique spin-doublet and we numerically perform the SWT as shown in the SI [51]. The system is ph-symmetric at $V_g = 0$ such that $W_{\alpha\beta} = 0$. We also find $J_{ss} = J_{dd} > 0$. Although J_{sd} is always finite, we find that its sign alternates for $M = 1, 3, 5, 7, \dots$. In particular, $J_{sd} < 0$ for $M = 3$ but $J_{sd} > 0$ for $M = 5$. One might anticipate that interpolating between $M = 3$ and $M = 5$ might yield a sweet spot solution where $J_{sd} = 0$. Avoiding odd loops and preserving sd symmetry, this can be achieved by connecting sites 1 to 4 and 2 to 5, viz:

$$H_{\text{mol}} = \frac{U}{2} \sum_{m=1}^{5} (\hat{n}_m - 1)^2 + t \sum_{\sigma} \sum_{m=1}^{4} \left(d_{m\sigma}^\dagger d_{m+1\sigma} + \text{H.c.} \right)$$
$$+ t' \sum_{\sigma} \left(d_{1\sigma}^\dagger d_{4\sigma} + d_{2\sigma}^\dagger d_{5\sigma} + \text{H.c.} \right) . \qquad (3)$$

For small t'/t we expect small perturbations to the $M = 5$ chain solution, whereas for large t'/t the next-next-nearest-neighbour tunneling provides a shortcut through the chain so that only 3 sites are needed to connect s and d leads. Numerical results of the SWT are presented in Fig. 1, together with a schematic illustration of the junction. At ph symmetry $V_g = 0$, the effective model parameters are plotted as a function of t'/t in the right panel. We indeed confirm that $j_{sd} = 0$ at a special value $t' = t'_c$ (black line). In the left panel we show the gate evolution of the same parameters at $t' = t'_c$, with the 2CK conditions being satisfied here at $V_g = 0$.

Non-perturbative solution: NRG.– To confirm the existence of a 2CK critical point in this simple 5-site molecular cluster, we turn to the non-perturbative solution of the full molecular junction involving Eq. 3 using NRG [60], where we set $t = \frac{1}{2}$ and the conduction electron bandwidth $D = 1$ from now on. Numerical results are presented in Fig. 2. In panel (a) we compare SWT predictions for the critical t'_c with those obtained by NRG for different interaction strengths U, showing excellent agreement. In particular, we note that the 2CK critical point can be realized for *any* finite U. Interestingly, we find that $t'_c \to t$ as $U \to 0$. The $U = 0$ limit of Eq. 3 is studied in the SI [51]: we find $t' = t$ is a singular point of the non-interacting model with strictly decoupled molecular degrees of freedom that give a finite $T = 0$ entropy and a QI-driven conductance node. With interactions switched on, the critical t'_c is no longer at t but we still find a residual $T = 0$ entropy and a conductance node – now characterizing the 2CK critical fixed point. Panel (c) shows the molecular contribution to the entropy S_{mol} as a function of T at the critical point for different V. The critical point can be realized for any combination of V and U (in panel (c) we take fixed U), and in all cases

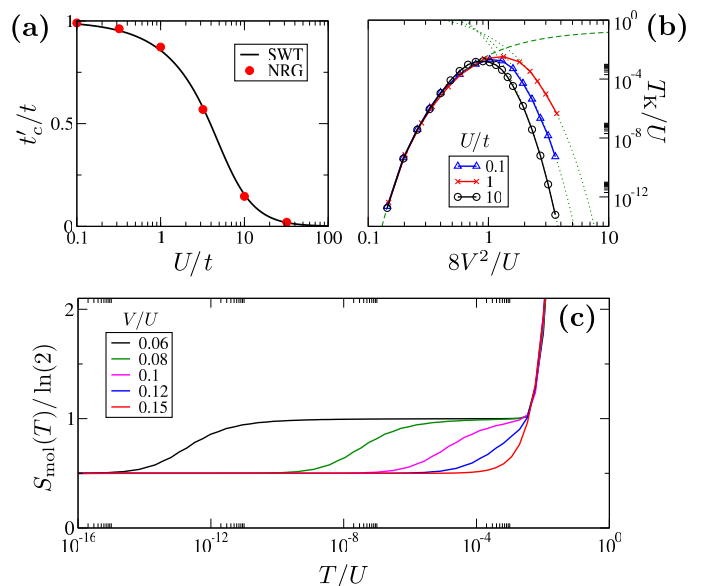FIG. 2. 2CK critical point driven by QI. (a) Critical coupling t'_c as a function of U/t, with NRG results (points) validating SWT predictions (line). (b) 2CK Kondo temperature T_K vs $8V^2/U \equiv J_K$ for different U/t obtained by NRG. Dashed line is $T_K/U \sim \exp[-4/J_K]$ valid for $J_K < 1$ whereas the dotted lines show $T_K/U \sim \exp[-aJ_K]$ with $a \equiv a(U) \sim \mathcal{O}(1)$ for $J_K > 1$. (c) Entropy S_{mol} vs T/U for different V/U at the 2CK critical point for $U/t = 10$, showing a residual $\frac{1}{2}\ln(2)$.

we find $S_{\text{mol}} = \frac{1}{2}\ln(2)$ for $T \ll T_K$, with T_K the critical Kondo temperature. This unusual value for the entropy is a hallmark of the free Majorana fermion localized on the molecule at low temperatures at the 2CK critical point [38, 50]. For small molecule-lead coupling, T_K is small and we have an extended intermediate $\ln(2)$ plateau corresponding to the local moment regime of Eq. 2. Remarkably however, at larger V the Kondo temperature can be boosted to large (non-universal) values and local moment physics is entirely eliminated. This scenario lies outside of the regime described by Eq. 2, suggesting that the interference giving rise to criticality is a topological feature of the geometry in Eq. 3. In Fig. 2(b) we plot the evolution of the Kondo temperature with $8V^2/U \equiv J_K$ (where J_K is the SWT Kondo coupling for a single Anderson impurity [47]), showing that a maximum value $T_K \sim 10^{-2}U$ can be realized for all values of U considered when $J_K \sim 1$. A weak-strong coupling duality [61] is found on further increasing J_K – see dashed and dotted lines in Fig. 2(b). Note that the critical point is a non-Fermi liquid and as such is not perturbatively connected to the $U = 0$ limit: even though the critical point can be realized at small U, we find that $T_K \to 0$ as $U \to 0$.

Gate control and entropy measurement.– With t' tuned to the 2CK critical point at t'_c, we can vary the gate voltage V_g in the vicinity of $V_g = 0$. This perturbation drives the system away from the 2CK fixed point and towards a standard Kondo strong-coupling Fermi liquid
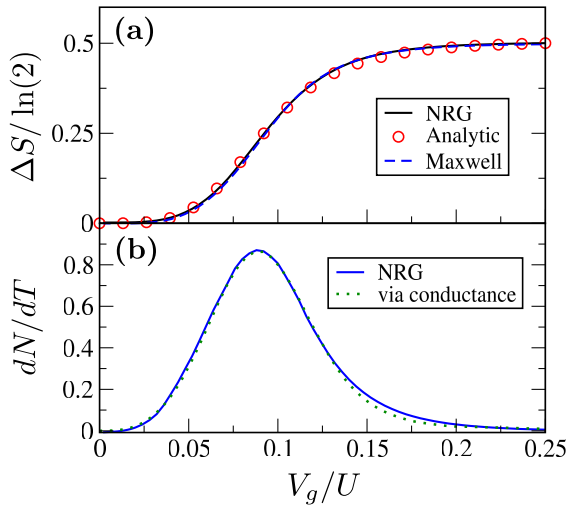
FIG. 3. (a) Entropy change ΔS as the molecular junction is driven away from the critical point by increasing gate voltage V_g. NRG results (line) compared with analytic result Eq. 5 (points). (b) dN/dT from NRG (line), compared with prediction via conductance from Eq. 7 (dotted line). Dashed line in the top panel obtained by integrating dN/dT over V_g. Plotted for $U/t = 10$, $V/U = 0.15$, $t' = t'_c$, $T = 10^{-6} \ll T_K$.

(FL) state on the scale of T^*. From NRG we find [51],

$$T^* \sim V_g^4 \qquad : \quad T^* \ll T_K \qquad (4)$$

which holds in the universal critical regime. Along this FL crossover, physical properties are universal scaling functions of T^*/T and hence $V_g/T^{1/4}$. For the pure 2CK model in this regime, bosonization methods give an exact result for the entropy change from the critical point [38],

$$\Delta S \left(\frac{T^*}{T} \right) = \frac{T^*}{T} \left[\psi \left(\frac{1}{2} + \frac{T^*}{T} \right) - 1 \right] - \ln \left[\frac{1}{\sqrt{\pi}} \Gamma \left(\frac{1}{2} + \frac{T^*}{T} \right) \right] \qquad (5)$$

with Γ (ψ) the gamma (digamma) function. The form of this crossover is entirely characteristic of the 2CK critical point [52]. Using Eq. 4, this crossover can be achieved by fixing T ($\ll T_K$) and detuning V_g (which controls T^*). This is shown in the top panel of Fig. 3, which compares NRG results for the junction (line) to Eq. 5 (points).

Recent progress has been made in observing entropic signatures in nanoelectronics experiments, by exploiting local Maxwell relations which connect the entropy change for a process to measureable changes in the charge [62–64]. Since the gate voltage V_g couples to the total molecule charge $\hat{N} = \sum_m \hat{n}_m$, the change in entropy induced by scanning V_g as in Fig. 3(a) follows as $\Delta S = - \int dV_g \, dN/dT$. The quantity dN/dT is shown in Fig. 3(b). Application of the Maxwell relation yields the blue-dashed line in Fig. 3(a), which agrees perfectly with the direct entropy calculation. We argue that the molecular system is well suited to this because T_K can be boosted to large values, meaning that the universal critical regime should be experimentally accessible.
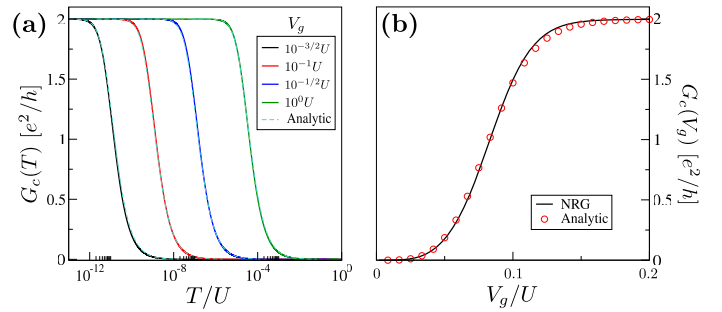

FIG. 4. Series conductance along the FL crossover (a) as a function of temperature for different gate voltages; and (b) as a function of gate voltage at fixed $T = 10^{-6} \ll T_K$; compared with Eq. 6. Shown for $U/t = 10$, $V/U = 0.15$, $t' = t'_c$.

Transport.– At the 2CK critical point, the series conductance through the molecular junction vanishes due to the many-body QI node. However, a nontrivial transport signature is picked up along the FL crossover by detuning the gate voltage. NRG results for the junction conductance $G_c(T)$ as a function of T at fixed detuning V_g are shown in Fig. 4(a). The maximum conductance of $2e^2/h$ for a single electron transistor is recovered at low temperatures $T \ll T^*$ in all cases. Fig. 4(b) shows the gate evolution of the conductance $G_c(V_g)$ at fixed T ($\ll T_K$), and is the analogous plot to Fig. 3(a).

The exact solution of the pure 2CK model along the FL crossover [38] yields a prediction for conductance [65],

$$G_c \left(\frac{T^*}{T} \right) = \frac{2e^2}{h} \times \left(\frac{T^*}{T} \right) \psi' \left(\frac{1}{2} + \frac{T^*}{T} \right) , \qquad (6)$$

where T^* depends on V_g via Eq. 4 and ψ' is the trigamma function. This expression matches essentially perfectly with NRG data for the full molecular junction in Fig. 4.

Finally, from the Maxwell relation $dN/dT = -dS/dV_g$ we can use Eqs. 4-6 to prove the exact conductance-charge relation [63] in the universal FL crossover regime,

$$\frac{dN}{dT} \sim \frac{V_g^3}{T} \left(1 - \frac{Gc(V_g, T)}{2e^2/h} \right) , \qquad (7)$$

meaning that experimental conductance data can be translated into dN/dT (see Fig. 3(b), dotted line) and then integrated to extract the entropy.

Inverse design.– The above results establish the existence of the QI-2CK effect in a simple molecular moiety with exact *ph* and *sd* symmetry. In a more general setting, however, we can use inverse design to search for candidate systems that satisfy the 2CK conditions. This can be done by setting up a loss function, for example $\mathcal{L} = j_{sd}^2 + w_{sd}^2 + (j_{ss} - j_{dd})^2$, which is minimum when the 2CK conditions on the effective model parameters are met. We then minimize this function with respect to the bare model parameters by gradient descent (GD). In practice this involves finding the derivatives of $j_{\alpha\beta}$ and
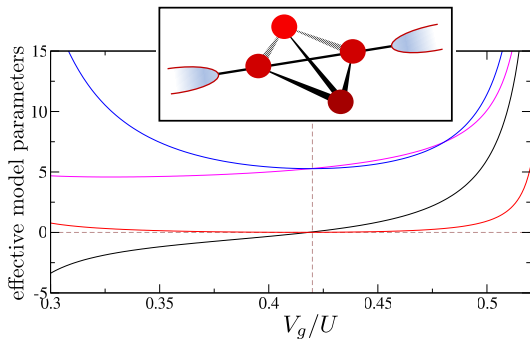
FIG. 5. Inverse design of a 4-site molecular junction using GD optimization of effective SWT parameters to realize the QI-2CK condition at gate voltage $V_g/U = 0.42$. Black: j_{sd}; red: w_{sd}; magenta: j_{ss}; blue: j_{dd}. Parameters given in [51].

$w_{\alpha\beta}$ with respect to t_{mn} and U_{mn}, which can be achieved using differentiable programming techniques [66]. In the SI [51] we show that this can be implemented very efficiently within our improved SWT scheme. Using this methodology, we could find a family of low-symmetry molecular junctions involving just 4 interacting sites [51], a representative example of which is shown in Fig. 5. By fine-tuning the gate voltage V_g in this structure we predict 2CK criticality. We did not find any 2CK critical systems involving 1, 2, or 3 sites.

A non-perturbative extension utilizing 'differentiable NRG' [67] to optimize bare model parameters directly via GD could be used to bypass the SWT approximation.

Conclusion.– The 2CK critical point can be realized by exploiting many-body QI effects in simple molecular junctions or coupled quantum dot devices, featuring a few tunnel-coupled, interacting orbitals. QI effects can be manipulated by tuning gate voltages to switch between a perfect node and perfect Kondo resonant transmission.

Inverse design can be used to search automatically for systems displaying desired functionality. The molecular moieties we identified are not intended to be atomistic models of any real molecule. However, the inverse design approach could be integrated with chemical databases to search for realistic candidate molecular junctions [68].

Our results open the door to designer devices utilizing many-body QI effects. For example, simple structures exhibiting three-channel Kondo [69] or two-impurity Kondo [70, 71] effects, or lattice extensions describing non-Fermi liquid materials [72]. Inverse design could be used to optimize performance of nanoscale transistors, rectifiers, spintronics devices and other quantum devices.

* Andrew.Mitchell@UCD.ie

[1] L. P. Kouwenhoven, D. Austing, and S. Tarucha, Few-electron quantum dots, Reports on progress in physics **64**, 701 (2001).

[2] R. Hanson, L. P. Kouwenhoven, J. R. Petta, S. Tarucha, and L. M. Vandersypen, Spins in few-electron quantum dots, Reviews of modern physics **79**, 1217 (2007).

[3] D. Goldhaber-Gordon, H. Shtrikman, D. Mahalu, D. Abusch-Magder, U. Meirav, and M. Kastner, Kondo effect in a single-electron transistor, Nature **391**, 156 (1998); S. M. Cronenwett, T. H. Oosterkamp, and L. P. Kouwenhoven, A tunable kondo effect in quantum dots, Science **281**, 540 (1998).

[4] J. Park, A. N. Pasupathy, J. I. Goldsmith, C. Chang, Y. Yaish, J. R. Petta, M. Rinkoski, J. P. Sethna, H. D. Abruña, P. L. McEuen, *et al.*, Coulomb blockade and the kondo effect in single-atom transistors, Nature **417**, 722 (2002); W. Liang, M. P. Shores, M. Bockrath, J. R. Long, and H. Park, Kondo resonance in a single-molecule transistor, *ibid.* **417**, 725 (2002).

[5] M. L. Perrin, E. Burzurí, and H. S. van der Zant, Single-molecule transistors, Chemical Society Reviews **44**, 902 (2015).

[6] A. R. Champagne, A. N. Pasupathy, and D. C. Ralph, Mechanically adjustable and electrically gated single-molecule transistors, Nano letters **5**, 305 (2005).

[7] B. Xu and N. J. Tao, Measurement of single-molecule resistance by repeated formation of molecular junctions, science **301**, 1221 (2003).

[8] J. Paaske, A. Rosch, P. Wölfle, N. Mason, C. Marcus, and J. Nygård, Non-equilibrium singlet–triplet kondo effect in carbon nanotubes, Nature physics **2**, 460 (2006).

[9] N. Roch, S. Florens, T. A. Costi, W. Wernsdorfer, and F. Balestro, Observation of the underscreened kondo effect in a molecular transistor, Physical review letters **103**, 197202 (2009).

[10] J. Parks, A. Champagne, T. Costi, W. Shum, A. Pasupathy, E. Neuscamman, S. Flores-Torres, P. Cornaglia, A. Aligia, C. Balseiro, *et al.*, Mechanical control of spin states in spin-1 molecules and the underscreened kondo effect, Science **328**, 1370 (2010).

[11] X. Guo, Q. Zhu, L. Zhou, W. Yu, W. Lu, and W. Liang, Evolution and universality of two-stage kondo effect in single manganese phthalocyanine molecule transistors, Nature communications **12**, 1566 (2021).

[12] C. A. Stafford, D. M. Cardamone, and S. Mazumdar, The quantum interference effect transistor, Nanotechnology **18**, 424014 (2007).

[13] C. M. Guédon, H. Valkenier, T. Markussen, K. S. Thygesen, J. C. Hummelen, and S. J. Van Der Molen, Observation of quantum interference in molecular charge transport, Nature nanotechnology **7**, 305 (2012).

[14] Y. Li, M. Buerkle, G. Li, A. Rostamian, H. Wang, Z. Wang, D. R. Bowler, T. Miyazaki, L. Xiang, Y. Asai, *et al.*, Gate controlling of quantum interference and direct observation of anti-resonances in single molecule charge transport, Nature materials **18**, 357 (2019).

[15] J. Bai, A. Daaoub, S. Sangtarash, X. Li, Y. Tang, Q. Zou, H. Sadeghi, S. Liu, X. Huang, Z. Tan, *et al.*, Anti-resonance features of destructive quantum interference in single-molecule thiophene junctions achieved by elec-

trochemical gating, Nature Materials **18**, 364 (2019).

[16] J. E. Greenwald, J. Cameron, N. J. Findlay, T. Fu, S. Gunasekaran, P. J. Skabara, and L. Venkataraman, Highly nonlinear transport across single-molecule junctions via destructive quantum interference, Nature Nanotechnology **16**, 313 (2021).

[17] A. K. Mitchell, K. G. Pedersen, P. Hedegård, and J. Paaske, Kondo blockade due to quantum interference in single-molecule junctions, Nature communications **8**, 1 (2017).

[18] N. Roch, S. Florens, V. Bouchiat, W. Wernsdorfer, and F. Balestro, Quantum phase transition in a single-molecule quantum dot, Nature **453**, 633 (2008).

[19] S. Florens, A. Freyn, N. Roch, W. Wernsdorfer, F. Balestro, P. Roura-Bas, and A. Aligia, Universal transport signatures in two-electron molecular quantum dots: gate-tunable hund's rule, underscreened kondo effect and quantum phase transitions, Journal of Physics: Condensed Matter **23**, 243202 (2011).

[20] E. Lörtscher, J. W. Ciszek, J. Tour, and H. Riel, Reversible and controllable switching of a single-molecule junction, Small **2**, 973 (2006).

[21] S. Y. Quek, M. Kamenetska, M. L. Steigerwald, H. J. Choi, S. G. Louie, M. S. Hybertsen, J. Neaton, and L. Venkataraman, Mechanically controlled binary conductance switching of a single-molecule junction, Nature nanotechnology **4**, 230 (2009).

[22] S. J. van der Molen and P. Liljeroth, Charge transport through molecular switches, Journal of Physics: Condensed Matter **22**, 133001 (2010).

[23] J. L. Zhang, J. Q. Zhong, J. D. Lin, W. P. Hu, K. Wu, G. Q. Xu, A. T. Wee, and W. Chen, Towards single molecule switches, Chemical Society Reviews **44**, 2998 (2015).

[24] M. Elbing, R. Ochs, M. Koentopp, M. Fischer, C. von Hänisch, F. Weigend, F. Evers, H. B. Weber, and M. Mayor, A single-molecule diode, Proceedings of the National Academy of Sciences **102**, 8815 (2005).

[25] M. L. Perrin, E. Galán, R. Eelkema, J. M. Thijssen, F. Grozema, and H. S. van der Zant, A gate-tunable single-molecule diode, Nanoscale **8**, 8919 (2016).

[26] A. Batra, P. Darancet, Q. Chen, J. S. Meisner, J. R. Widawsky, J. B. Neaton, C. Nuckolls, and L. Venkataraman, Tuning rectification in single-molecular diodes, Nano letters **13**, 6233 (2013).

[27] I. Díez-Pérez, J. Hihath, Y. Lee, L. Yu, L. Adamska, M. A. Kozhushner, I. I. Oleynik, and N. Tao, Rectification and stability of a single molecular diode with controlled orientation, Nature chemistry **1**, 635 (2009).

[28] R. M. Metzger, Unimolecular electrical rectifiers, Chemical reviews **103**, 3803 (2003).

[29] R. Gupta, J. A. Fereiro, A. Bayat, A. Pritam, M. Zharnikov, and P. C. Mondal, Nanoscale molecular rectifiers, Nature Reviews Chemistry **7**, 106 (2023).

[30] E. M. Dief, P. J. Low, I. Díez-Pérez, and N. Darwish, Advances in single-molecule junctions as tools for chemical and biochemical analysis, Nature Chemistry , 1 (2023).

[31] N. Xin, J. Guan, C. Zhou, X. Chen, C. Gu, Y. Li, M. A. Ratner, A. Nitzan, J. F. Stoddart, and X. Guo, Concepts in the design and engineering of single-molecule electronic devices, Nature Reviews Physics **1**, 211 (2019).

[32] L. Kouwenhoven, Coupled quantum dots as artificial molecules, Science **268**, 1440 (1995).

[33] H. Jeong, A. M. Chang, and M. R. Melloch, The kondo effect in an artificial quantum dot molecule, Science **293**, 2221 (2001).

[34] R. P. Feynman, There's plenty of room at the bottom, Feynman and computation **63**, 76 (2018).

[35] P. Barthelemy and L. M. Vandersypen, Quantum dot systems: a versatile platform for quantum simulations, Annalen der Physik **525**, 808 (2013).

[36] I. Affleck and A. W. Ludwig, Universal noninteger "ground-state degeneracy" in critical quantum systems, Physical Review Letters **67**, 161 (1991).

[37] P. Nozieres and A. Blandin, Kondo effect in real metals, Journal de Physique **41**, 193 (1980).

[38] V. Emery and S. Kivelson, Mapping of the two-channel kondo problem to a resonant-level model, Physical Review B **46**, 10812 (1992).

[39] Y. Komijani, Isolating kondo anyons for topological quantum computation, Physical Review B **101**, 235131 (2020).

[40] M. Lotem, E. Sela, and M. Goldstein, Manipulating non-abelian anyons in a chiral multichannel kondo model, Physical Review Letters **129**, 227703 (2022).

[41] P. L. Lopes, I. Affleck, and E. Sela, Anyons in multichannel kondo systems, Physical Review B **101**, 085141 (2020).

[42] R. Potok, I. Rau, H. Shtrikman, Y. Oreg, and D. Goldhaber-Gordon, Observation of the two-channel kondo effect, Nature **446**, 167 (2007).

[43] A. Keller, L. Peeters, C. Moca, I. Weymann, D. Mahalu, V. Umansky, G. Zaránd, and D. Goldhaber-Gordon, Universal fermi liquid crossover and quantum criticality in a mesoscopic system, Nature **526**, 237 (2015).

[44] Z. Iftikhar, S. Jezouin, A. Anthore, U. Gennser, F. Parmentier, A. Cavanna, and F. Pierre, Two-channel kondo effect and renormalization flow with macroscopic quantum charge states, Nature **526**, 233 (2015).

[45] Y. Oreg and D. Goldhaber-Gordon, Two-channel kondo effect in a modified single electron transistor, Phys. Rev. Lett. **90**, 136602 (2003).

[46] A. Furusaki and K. Matveev, Theory of strong inelastic cotunneling, Physical Review B **52**, 16676 (1995).

[47] A. Hewson, *The Kondo Problem to Heavy Fermions* (Cambridge University Press, Cambridge, England, 1993).

[48] J. R. Schrieffer and P. A. Wolff, Relation between the anderson and kondo hamiltonians, Physical Review **149**, 491 (1966); S. Bravyi, D. P. DiVincenzo, and D. Loss, Schrieffer–wolff transformation for quantum many-body systems, Annals of physics **326**, 2793 (2011).

[49] J. B. Rigo and A. K. Mitchell, Machine learning effective models for quantum systems, Physical Review B **101**, 241105 (2020).

[50] I. Affleck and A. W. Ludwig, Exact conformal-field-theory results on the multichannel kondo effect: Single-fermion green's function, self-energy, and resistivity, Physical Review B **48**, 7297 (1993).

[51] See supplementary material.

[52] E. Sela, A. K. Mitchell, and L. Fritz, Exact crossover green function in the two-channel and two-impurity kondo models, Phys. Rev. Lett. **106**, 147202 (2011); A. K. Mitchell and E. Sela, Universal low-temperature crossover in two-channel kondo models, Phys. Rev. B **85**, 235127 (2012).

[53] C. Lambert, Basic concepts of quantum interference and electron transport in single-molecule electronics, Chemi-

cal Society Reviews **44**, 875 (2015).

[54] K. G. Pedersen, M. Strange, M. Leijnse, P. Hedegård, G. C. Solomon, and J. Paaske, Quantum interference in off-resonant transport through single molecules, Physical Review B **90**, 125413 (2014).

[55] E. R. Gagliano, E. Dagotto, A. Moreo, and F. C. Alcaraz, Correlation functions of the antiferromagnetic heisenberg model using a modified lanczos method, Physical Review B **34**, 1677 (1986).

[56] U. Schollwöck, The density-matrix renormalization group in the age of matrix product states, Annals of physics **326**, 96 (2011).

[57] D. Zgid, E. Gull, and G. K.-L. Chan, Truncated configuration interaction expansions as solvers for correlated quantum impurity models and dynamical mean-field theory, Physical Review B **86**, 165128 (2012).

[58] C. Coulson and G. Rushbrooke, Note on the method of molecular orbitals, in *Mathematical Proceedings of the Cambridge Philosophical Society*, Vol. 36 (Cambridge University Press, 1940) pp. 193–200.

[59] Y. Tsuji, E. Estrada, R. Movassagh, and R. Hoffmann, Quantum interference, graphs, walks, and polynomials, Chemical reviews **118**, 4887 (2018).

[60] K. G. Wilson, The renormalization group: Critical phenomena and the kondo problem, Reviews of modern physics **47**, 773 (1975); R. Bulla, T. A. Costi, and T. Pruschke, Numerical renormalization group method for quantum impurity systems, Reviews of Modern Physics **80**, 395 (2008).

[61] C. Kolf and J. Kroha, Strong versus weak coupling duality and coupling dependence of the kondo temperature in the two-channel kondo model, Physical Review B **75**, 045129 (2007).

[62] N. Hartman, C. Olsen, S. Lüscher, M. Samani, S. Fallahi, G. C. Gardner, M. Manfra, and J. Folk, Direct entropy measurement in a mesoscopic quantum system, Nature Physics **14**, 1083 (2018).

[63] C. Han, Z. Iftikhar, Y. Kleeorin, A. Anthore, F. Pierre, Y. Meir, A. K. Mitchell, and E. Sela, Fractional entropy of multichannel kondo systems from conductance-charge relations, Physical Review Letters **128**, 146803 (2022).

[64] T. Child, O. Sheekey, S. Lüscher, S. Fallahi, G. C. Gardner, M. Manfra, A. Mitchell, E. Sela, Y. Kleeorin, Y. Meir, *et al.*, Entropy measurement of a strongly coupled quantum dot, Physical Review Letters **129**, 227702 (2022).

[65] A. K. Mitchell, L. A. Landau, L. Fritz, and E. Sela, Universality and scaling in a charge two-channel kondo device, Phys. Rev. Lett. **116**, 157202 (2016).

[66] M. Bartholomew-Biggs, S. Brown, B. Christianson, and L. Dixon, Automatic differentiation of algorithms, Journal of Computational and Applied Mathematics **124**, 171 (2000).

[67] J. B. Rigo and A. K. Mitchell, Automatic differentiable numerical renormalization group, Physical Review Research **4**, 013227 (2022).

[68] S. Raghunathan and U. D. Priyakumar, Molecular representations for machine learning applications in chemistry, International Journal of Quantum Chemistry **122**, e26870 (2022).

[69] Z. Iftikhar, A. Anthore, A. Mitchell, F. Parmentier, U. Gennser, A. Ouerghi, A. Cavanna, C. Mora, P. Simon, and F. Pierre, Tunable quantum criticality and superballistic transport in a "charge" kondo circuit, Science **360**, 1315 (2018).

[70] B. Jones, C. Varma, and J. Wilkins, Low-temperature properties of the two-impurity kondo hamiltonian, Physical review letters **61**, 125 (1988).

[71] W. Pouse, L. Peeters, C. L. Hsueh, U. Gennser, A. Cavanna, M. A. Kastner, A. K. Mitchell, and D. Goldhaber-Gordon, Quantum simulation of an exotic quantum critical point in a two-site charge kondo circuit, Nature Physics **19**, 492 (2023).

[72] D. Cox and M. Jarrell, The two-channel kondo route to non-fermi-liquid metals, Journal of Physics: Condensed Matter **8**, 9825 (1996).

Supplementary Material

Many-body quantum interference route to the two-channel Kondo effect: Inverse design for molecular junctions

Sudeshna Sen[1] and Andrew K. Mitchell[2, 3]

[1] *Department of Physics, IIT(ISM) Dhanbad, Dhanbad-826004, Jharkhand, India*
[2] *School of Physics, University College Dublin, Belfield, Dublin 4, Ireland*
[3] *Centre for Quantum Engineering, Science, and Technology, University College Dublin, Ireland*

S-I. MICROSCOPIC MODELS OF MOLECULAR JUNCTIONS

We describe molecular junctions (and coupled quantum dot devices constituting artificial molecular junctions) in terms of generalized quantum impurity models of the type,

$$\hat{H} = \hat{H}_{\text{mol}} + \hat{H}_{\text{leads}} + \hat{H}_{\text{hyb}} + \hat{H}_{\text{gate}} \qquad \text{(S-1)}$$

where the part of the Hamiltonian $\hat{H}_{\text{mol}}$ describing the isolated molecule is given by an extended Hubbard model,

$$\hat{H}_{\text{mol}} = \sum_{\sigma=\uparrow,\downarrow} \sum_{m,n} t_{mn} d^\dagger_{m\sigma} d_{n\sigma} + \tfrac{1}{2} \sum_{m,n} U_{mn} \hat{n}_m \hat{n}_n \quad \text{(S-2)}$$

as given in Eq. 1 of the main text. Here $d^{(\dagger)}_{m\sigma}$ annihilates (creates) an electron on molecule orbital m with spin σ and $\hat{n}_m = \sum_\sigma \hat{n}_{m\sigma}$ is the total number operator for orbital m, where $\hat{n}_{m\sigma} = d^\dagger_{m\sigma} d_{m\sigma}$. The single-particle tunneling matrix elements between orbitals $m \neq n$ are given by t_{mn} $(= t^*_{nm})$ whereas the onsite potentials are $\epsilon_m = t_{mm} + \tfrac{1}{2} U_{mm}$. The term U_{mn} $(= U_{nm})$ embodies electronic interactions on the molecule. The standard local Hubbard interaction term $U_m \hat{n}_{m\uparrow} \hat{n}_{m\downarrow}$ between up and down spin electrons on a given site m is already included in the diagonal part of the second term of Eq. S-2, with $U_m \equiv U_{mm}$. The off-diagonal parts U_{mn} for $m \neq n$ correspond to capacitive (Coulomb) repulsion between different sites. In principle one can also add spin-orbit coupling terms, anisotropies, and exchange interactions. The formalism presented below can be straightforwardly adapted to treat any $\hat{H}_{\text{mol}}$.

The source $(\alpha = s)$ and drain $(\alpha = d)$ leads are taken to be thermal reservoirs of non-interacting conduction electrons, $\hat{H}_{\text{leads}} = \sum_\alpha \hat{H}^\alpha_{\text{leads}}$ with

$$\hat{H}^\alpha_{\text{leads}} = \sum_{k,\sigma} \epsilon_k c^\dagger_{\alpha k \sigma} c_{\alpha k \sigma} \qquad \text{(S-3)}$$

where for simplicity we take the dispersion ϵ_k to be independent of spin σ and equivalent for both leads α (although again this can be straightforwardly generalized without affecting the following).

The molecule frontier orbital $d_{r_\alpha \sigma}$ couples to the conduction electrons of lead α according to the hybridization term

$$\hat{H}_{\text{hyb}} = \sum_{\alpha,k,\sigma} V_{\alpha k} (d^\dagger_{r_\alpha \sigma} c_{\alpha k \sigma} + \text{H.c.}) \ . \qquad \text{(S-4)}$$

We now define the local lead orbitals at the molecule position as $c_{\alpha\sigma} = \frac{1}{V_\alpha} \sum_k V_{\alpha k} c_{\alpha\sigma k}$ with $V_\alpha^2 = \sum_k V^2_{\alpha k}$ such that $\hat{H}_{\text{hyb}} = \sum_{\alpha,\sigma} V_\alpha (d^\dagger_{r_\alpha \sigma} c_{\alpha\sigma} + \text{H.c.})$.

The free lead density of states at the junction position (taken to the same for both leads and independent of spin) is $\rho(\omega) = -\frac{1}{\pi} \text{Im} \ G^0_{\text{lead}}(\omega)$ where $G^0_{\text{lead}}(\omega) = \langle\langle c_{\alpha\sigma} ; c^\dagger_{\alpha\sigma} \rangle\rangle$ is the free Green's function for the local lead orbital $c_{\alpha\sigma}$ to which the molecule couples. For simplicity we use $\rho(\omega) = \rho_0 \theta(D - |\omega|)$ such that the lead density of states is constant $\rho_0 = 1/2D$ in a band of half-width D. Throughout this work we set $D = 1$.

The gate voltage V_g allows to tune the number of electrons on the molecule via $\hat{H}_{\text{gate}} = V_g \sum_m \hat{n}_m$.

A.   Interacting nanowire (Hubbard chains)

In the main text we discuss a particular limiting case of Eq. S-2 corresponding to an M-site 1d Hubbard chain,

$$\hat{H}_{\text{mol}} = t \sum_{m=1}^{M-1} \sum_\sigma \left(d^\dagger_{m\sigma} d_{m+1\sigma} + \text{H.c.} \right) + \sum_{m=1}^{M} \left(\epsilon \hat{n}_m + U \hat{n}_{m\uparrow} \hat{n}_{m\downarrow} \right) \tag{S-5}$$

which describes an interacting nanowire (for example the π-system of a conjugated hydrocarbon polymer [1]). We take constant nearest-neighbour tunneling t, constant onsite potentials ϵ and constant local Hubbard repulsion U. The source and drain leads are connected to the ends of the nanowire at sites $r_s = 1$ and $r_d = M$, such that

$$H_{\text{hyb}} = \sum_\sigma \left(V_s \, c^\dagger_{s\sigma} d_{1\sigma} + V_d \, c^\dagger_{d\sigma} d_{M\sigma} + \text{H.c.} \right) \ . \tag{S-6}$$

The low-energy effective model for this system with odd chain length M is discussed below in Sec. S-II B.

B.   Symmetric 5-site cluster

Introducing additional tunnel-couplings between different sites of the above 1d Hubbard chain clearly produces greater complexity and, in particular, more possibilities for QI effects.

However, if we want exact *ph* symmetry then the molecule connectivity must be compatible with a bipartite graph – which in the present context simply means that there should not be any odd-membered loops. The simplest system with an odd total number of sites with *sd*-symmetry to contain multiple paths through the molecule, while also realizing exact particle hole symmetry at $V_g = 0$, is the $M = 5$ chain with next-next-nearest-neighbour tunneling connecting sites $1 \leftrightarrow 4$ and $2 \leftrightarrow 5$,

$$
\begin{aligned}
H_{\mathrm{mol}} = \sum_{m=1}^{5} & \left(-\tfrac{1}{2}U\hat{n}_m + U\hat{n}_{m\uparrow}\hat{n}_{m\downarrow} \right) \\
& + t \sum_{m=1}^{4} \sum_{\sigma} \left(d_{m\sigma}^{\dagger}d_{m+1\sigma} + \text{H.c.} \right) \\
& + t' \sum_{\sigma} \left(d_{1\sigma}^{\dagger}d_{4\sigma} + d_{2\sigma}^{\dagger}d_{5\sigma} + \text{H.c.} \right)
\end{aligned} \tag{S-7}
$$

which is equivalent to Eq. 3 of the main text. We attach leads to sites 1 and 5 via Eq. S-6. We discuss the low-energy effective model for this system below in Sec. S-II C.

C. Low-symmetry 4-site cluster

Finally we consider a general low-symmetry structure with just $M = 4$ interacting sites. We simplify to local Hubbard interactions:

$$
\hat{H}_{\mathrm{mol}} = \sum_{m,n} \sum_{\sigma} t_{mn} d_{m\sigma}^{\dagger} d_{n\sigma} + \sum_m U_m \hat{n}_{m\uparrow}\hat{n}_{m\downarrow} \tag{S-8}
$$

Leads are attached to sites 1 and 4 via Eq. S-6. We discuss gradient descent optimization of this system to satisfy the QI-2CK conditions in Sec. S-VII A.

The parameters used in Fig. 5 of the main text are $t_{11} \simeq 0.697$, $t_{22} \simeq 0.642$, $t_{33} \simeq 0.480$, $t_{44} \simeq 0.253$, $V_g = 0.42$, $t_{12} \simeq 0.102$, $t_{13} \simeq 0.053$, $t_{14} \simeq 0.1$, $t_{23} \simeq 0.109$, $t_{24} \simeq 0.046$, $t_{34} \simeq 0.169$.

S-II. GENERALIZED NUMERICAL SCHRIEFFER-WOLFF TRANSFORMATION

The Schrieffer-Wolff transformation (SWT) was first applied to the mapping between the Anderson impurity model (AIM) and the Kondo model [2]. For the AIM it involves projecting onto the impurity spin states by eliminating virtual excitations and folding in their contribution to effective model parameters. The SWT is in essence a single-step renormalisation group (RG) procedure. Typically the mapping is done perturbatively to second order in the impurity-bath hybridization, which is then equivalent to performing second-order Brillouin-Wigner perturbation theory (BWPT) [3]. For the AIM-to-Kondo mapping this can be done straightforwardly and analytic expressions for the Kondo model parameters are easily obtained.

However, in the present context of complex molecular junctions, an exact analytic treatment of the SWT is in general not possible, and we must resort to a *numerical* evaluation of the effective model parameters [4, 5]. Such a generalized numerical SWT is an ideal tool for efficiently describing many-body quantum interference (QI) effects. It can also be integrated with machine learning (ML) algorithms for inverse design, by identifying candidate molecular junctions that have specific desired effective model properties, as shown below.

Before proceeding we make a comment on the validity of the SWT. The RG character of quantum impurity systems means that a second-order SWT typically yields the correct operator structure of the low-energy effective model, even if the precise value of the derived parameters is not exact [6]. However, even infinite-order SWT [7] neglects retardation effects from the conduction electrons resulting in bandwidth renormalization [8], and more sophisticated non-perturbative techniques such as the numerical renormalization group [9] (NRG) are ultimately required. On the other hand, in this work we demonstrate that QI effects are very well captured by SWT (even quantitatively) when compared with NRG.

A. Formalism

In this work we are interested in deriving generalized two-channel Kondo (2CK) models of the type Eq. 2 from the main paper. Such a description arises in two-lead molecular junctions as the low-energy effective model when the isolated molecule ground state manifold comprises a unique spin-doublet [4, 5]. The structure of the effective model is constrained by $U(1)$ charge conservation and $SU(2)$ spin symmetry. The spin-doublet ground state of the molecule implies that the ground state hosts an odd number N of electrons, and that tunneling to and from the leads involves $N \pm 1$ even-electron sectors with integer spin.

With $\hat{H}'_{\mathrm{mol}} = \hat{H}_{\mathrm{mol}} + \hat{H}_{\mathrm{gate}}$ taken to include gate voltage effects on the isolated molecule, we define a set of exact eigenstates $\{|\psi_j^{n;S^z}\rangle\}$ satisfying the Schrödinger equation $\hat{H}'_{\mathrm{mol}}|\psi_j^{n;S^z}\rangle = E_j^{n;S^z}|\psi_j^{n;S^z}\rangle$, where n is the number of electrons on the isolated molecule, S^z is the total molecule spin projection, and j is an index distinguishing molecule states with the same n and S^z. The ground spin doublet states are specified by $|\psi_0^{N;\sigma}\rangle$ with $\sigma = \uparrow, \downarrow$, and the corresponding ground state energy is $E_{\mathrm{gs}} \equiv E_0^{N;\uparrow} = E_0^{N;\downarrow}$.

Eigenstates of $\hat{H}'_{\mathrm{mol}}$ can be expressed in the (computational) many-body product-state basis $\{|\phi_k^{n;S^z}\rangle\}$, which are labelled by the same quantum numbers, viz:

$$
|\psi_j^{n;S^z}\rangle = \sum_k U_{k,j}^{n;S^z} |\phi_k^{n;S^z}\rangle . \tag{S-9}
$$

For notational convenience we define product basis vectors $\vec{\phi}^{n,S^z} = \left(|\phi_0^{n;S^z}\rangle, |\phi_1^{n;S^z}\rangle, |\phi_2^{n;S^z}\rangle, ... \right)$ and eigen-

basis vectors $\vec{\psi}^{n,S^z} = \left(|\psi_0^{n;S^z}\rangle, |\psi_1^{n;S^z}\rangle, |\psi_2^{n;S^z}\rangle, ... \right)$. These are related by Eq. S-9 as $\vec{\psi}^{n,S^z} = \vec{\phi}^{n,S^z} U^{n;S^z}$ in terms of the transformation matrices $U^{n;S^z}$ with elements $U_{k,j}^{n;S^z}$. The Hamiltonian matrix for the isolated but interacting molecule in the computational product basis of a given quantum number subspace can then be written as $H_\phi^{n;S^z} = \left(\vec{\phi}^{n,S^z} \right)^\dagger \hat{H}'_{\text{mol}} \; \vec{\phi}^{n,S^z}$, whereas in the eigenbasis we have $H_\psi^{n;S^z} = \left(\vec{\psi}^{n,S^z} \right)^\dagger \hat{H}'_{\text{mol}} \; \vec{\psi}^{n,S^z} = \left(U^{n;S^z} \right)^\dagger H_\phi^{n;S^z} U^{n;S^z} \equiv \text{diag} \left(E_0^{n,S^z}, E_1^{n,S^z}, E_2^{n,S^z}, ... \right)$. These expressions hold separately in each subspace.

Finally, we will find it useful to define the vector of expansion coefficients for the N-electron *ground state* with spin σ as $\vec{U}_{\text{gs}}^{N;\sigma} = \left(U_{0,0}^{N;\sigma}, U_{1,0}^{N;\sigma}, U_{2,0}^{N;\sigma}, ... \right)^T$ such that $|\psi_0^{N;\sigma}\rangle = \vec{\phi}^{N;\sigma} \cdot \vec{U}_{\text{gs}}^{N;\sigma}$. We may also denote $\vec{\phi}_{\text{gs}} \equiv \vec{\phi}^{N;\uparrow}$ and $|\psi_{\text{gs}}\rangle \equiv |\psi_0^{N;\uparrow}\rangle$ and $\vec{U}_{\text{gs}} \equiv \vec{U}_{\text{gs}}^{N;\uparrow}$ for notational compactness where applicable.

With the above preliminaries established, we now use BWPT to project the full Hamiltonian $\hat{H} = \hat{H}_{\text{leads}} + \hat{H}'_{\text{mol}} + \hat{H}_{\text{hyb}}$ onto the low-energy manifold containing the spin-doublet molecule ground states, by perturbatively eliminating excitations to higher-lying molecule states. We define the projector $\hat{P} = \sum_{\sigma=\uparrow,\downarrow} |\psi_0^{N,\sigma}\rangle\langle\psi_0^{N,\sigma}|$ for the ground states to be kept and $\hat{Q} = \hat{1} - \hat{P}$ for the excited states to be discarded in our effective model. To second order in $\hat{H}_{\text{hyb}}$ we obtain an effective Hamiltonian,

$$\hat{H}_{\text{eff}} = \hat{P}\hat{H}\hat{P} + \hat{P}\hat{H}_{\text{hyb}}\hat{Q}(E_{\text{gs}} - \hat{H}'_{\text{mol}})^{-1}\hat{Q}\hat{H}_{\text{hyb}}\hat{P} . \quad \text{(S-10)}$$

With the specific form of the hybridization Hamiltonian,

$$\hat{H}_{\text{hyb}} = \sum_{\substack{s=\uparrow,\downarrow \\ \alpha=s,d}} V_\alpha \left(c_{\alpha s}^\dagger d_{r_\alpha s} + d_{r_\alpha s}^\dagger c_{\alpha s} \right) , \quad \text{(S-11)}$$

the effective model takes the form,

$$\hat{H}_{\text{eff}} = \hat{H}_{\text{leads}} + \sum \left(V_\alpha V_\beta \; A_{\substack{s,s' \\ \alpha,\beta}}^{\sigma\sigma'} \right) c_{\beta s'}^\dagger c_{\alpha s} |\psi_0^{N;\sigma'}\rangle\langle\psi_0^{N;\sigma}| , \quad \text{(S-12)}$$

where a sum over all indices of the tensor A is implied. Charge conservation, $SU(2)$ spin symmetry and Hermiticity impose constraints on the the tensor A. Together with the definitions,

$$\hat{\mathbb{S}}^+ = |\psi_0^{N;\uparrow}\rangle\langle\psi_0^{N;\downarrow}| \quad \text{(S-13)}$$

$$\hat{\mathbb{S}}^- = |\psi_0^{N;\downarrow}\rangle\langle\psi_0^{N;\uparrow}| \quad \text{(S-14)}$$

$$\hat{\mathbb{S}}^z = \tfrac{1}{2} \left[|\psi_0^{N;\uparrow}\rangle\langle\psi_0^{N;\uparrow}| - |\psi_0^{N;\downarrow}\rangle\langle\psi_0^{N;\downarrow}| \right] \quad \text{(S-15)}$$

for the retained molecule states and

$$\hat{\vec{s}}_{\alpha\beta} = \tfrac{1}{2} \sum_{ss'} c_{\beta s'}^\dagger \vec{\sigma}_{s's} \, c_{\alpha s} , \quad \text{(S-16)}$$

for the conduction electrons, we obtain the effective generalized 2CK model [4, 5], Eq. 2 of the main paper:

$$\hat{H}_{\text{eff}} = \hat{H}_{\text{leads}} + \sum_{\alpha\beta} \left[J_{\alpha\beta} \, \hat{\vec{\mathbb{S}}} \cdot \hat{\vec{s}}_{\alpha\beta} + W_{\alpha\beta} \sum_\sigma c_{\beta\sigma}^\dagger c_{\alpha\sigma} \right] . \quad \text{(S-17)}$$

In the following we consider the rescaled couplings $j_{\alpha\beta}$ and $w_{\alpha\beta}$ defined by $J_{\alpha\beta} = V_\alpha V_\beta j_{\alpha\beta}$ and $W_{\alpha\beta} = V_\alpha V_\beta w_{\alpha\beta}$, which follow from the factorized form of the couplings up to second order in Eq. S-12. It immediately follows that:

$$j_{\alpha\beta} = 2 \left(A_{\substack{\uparrow\uparrow \\ \alpha,\beta}}^{\uparrow\uparrow} - A_{\substack{\downarrow\downarrow \\ \alpha,\beta}}^{\uparrow\uparrow} \right) \quad \text{(S-18)}$$

$$w_{\alpha\beta} = \tfrac{1}{2} \left(A_{\substack{\uparrow\uparrow \\ \alpha,\beta}}^{\uparrow\uparrow} + A_{\substack{\downarrow\downarrow \\ \alpha,\beta}}^{\uparrow\uparrow} \right) \quad \text{(S-19)}$$

in terms of the amplitudes appearing in Eq. S-12. There are other equivalent forms which follow from the symmetry transformations but we shall use these ones.

The final step is of course to calculate the amplitudes A. This is done by inserting Eq. S-11 into Eq. S-10 and comparing with Eq. S-12. The amplitudes decompose into particle and hole tunneling processes

$$A_{\substack{s,s' \\ \alpha,\beta}}^{\sigma\sigma'} = p_{\substack{s,s' \\ \alpha,\beta}}^{\sigma\sigma'} - h_{\substack{s,s' \\ \alpha,\beta}}^{\sigma\sigma'} \quad \text{(S-20)}$$

where

$$p_{\substack{s,s' \\ \alpha,\beta}}^{\sigma\sigma'} = \sum_j \frac{\langle\psi_0^{N;\sigma'}|d_{r_\beta s'}|\psi_j^{N+1;\sigma+s}\rangle\langle\psi_j^{N+1;\sigma+s}|d_{r_\alpha s}^\dagger|\psi_0^{N;\sigma}\rangle}{E_{\text{gs}} - E_j^{N+1;\sigma+s}} \quad \text{(S-21)}$$

for the particle process and

$$h_{\substack{s,s' \\ \alpha,\beta}}^{\sigma\sigma'} = \sum_j \frac{\langle\psi_0^{N;\sigma'}|d_{r_\beta s'}^\dagger|\psi_j^{N-1;\sigma-s}\rangle\langle\psi_j^{N-1;\sigma-s}|d_{r_\alpha s}|\psi_0^{N;\sigma}\rangle}{E_{\text{gs}} - E_j^{N-1;\sigma-s}} \quad \text{(S-22)}$$

for the hole process. Note that spin conservation requires $\sigma + s = \sigma' + s'$ for particle tunneling and $\sigma - s = \sigma' - s'$ for hole tunneling.

Numerical calculations can be made dramatically more efficient by exploiting the following observation: we may express particle and hole amplitudes in matrix form, viz:

$$p_{\substack{s,s' \\ \alpha,\beta}}^{\sigma\sigma'} = \left[\left(X_{\beta s'+}^{N;\sigma'} \right)^\dagger \left[E_{\text{gs}} I - H_\psi^{N+1;\sigma+s} \right]^{-1} \left(X_{\alpha s+}^{N;\sigma} \right) \right]_{00} \quad \text{(S-23)}$$

$$h_{\substack{s,s' \\ \alpha,\beta}}^{\sigma\sigma'} = \left[\left(X_{\beta s'-}^{N;\sigma'} \right)^\dagger \left[E_{\text{gs}} I - H_\psi^{N-1;\sigma-s} \right]^{-1} \left(X_{\alpha s-}^{N;\sigma} \right) \right]_{00} \quad \text{(S-24)}$$

where $X_{\alpha s\pm}^{N;\sigma} = \left(\vec{\psi}^{N\pm1,\sigma\pm s} \right)^\dagger d_{r_\alpha s}^{(\dagger)} \; \vec{\psi}^{N;\sigma}$ is evaluated in the eigenbasis. Switching now to the product basis, we

write $\boldsymbol{X}^{N;\sigma}_{\alpha s\pm} = \left(\boldsymbol{U}^{N\pm1;\sigma\pm s}\right)^{\dagger} \mathbb{X}^{N;\sigma}_{\alpha s\pm} \, \boldsymbol{U}^{N;\sigma}$, where $\mathbb{X}^{N;\sigma}_{\alpha s\pm} = \left(\vec{\phi}^{N\pm1,\sigma\pm s}\right)^{\dagger} d^{(\dagger)}_{r_\alpha s} \, \vec{\phi}^{N;\sigma}$.

Inserting into Eqs. S-23 and S-24 we finally obtain,

$$p^{\sigma\sigma'}_{\substack{s,s' \\ \alpha,\beta}} = \left(\vec{U}^{N;\sigma'}_{\rm gs}\right)^{\dagger} \mathbb{M}^{\sigma\sigma'}_{\substack{s,s' \\ \alpha,\beta}}(+) \, \vec{U}^{N;\sigma}_{\rm gs} \qquad (\text{S-25})$$

$$h^{\sigma\sigma'}_{\substack{s,s' \\ \alpha,\beta}} = \left(\vec{U}^{N;\sigma'}_{\rm gs}\right)^{\dagger} \mathbb{M}^{\sigma\sigma'}_{\substack{s,s' \\ \alpha,\beta}}(-) \, \vec{U}^{N;\sigma}_{\rm gs} \qquad (\text{S-26})$$

with

$$\mathbb{M}^{\sigma\sigma'}_{\substack{s,s' \\ \alpha,\beta}}(\pm) = \left(\mathbb{X}^{N;\sigma'}_{\beta s'\pm}\right)^{\dagger} \left[E_{\rm gs}\boldsymbol{I} - \boldsymbol{H}^{N\pm1;\sigma\pm s}_\phi\right]^{-1} \left(\mathbb{X}^{N;\sigma}_{\alpha s\pm}\right) \qquad (\text{S-27})$$

and where $\vec{U}^{N;\sigma}_{\rm gs}$ is the vector of expansion coefficients for the *ground state* wavefunction only, as above.

The beauty of Eqs. S-25, S-26, S-27 is that only the *ground* eigenstate $|\psi^{N;\sigma}_0\rangle$ and the ground state energy $E_{\rm gs}$ of the isolated molecule are required: one does *not* need to fully diagonalize the entire molecule. The matrix $\mathbb{M}$ is simply evaluated in the original product basis. This is highly efficient since one can use eigensolvers targeting just the ground state for the calculation, meaning that large systems can be dealt with cheaply. This in turn permits high throughput calculations which can be integrated within ML routines for inverse design.

Although the above formulation is entirely general, we note from Eqs. S-18, S-19 that in the present context, the 2CK mapping requires only a few elements of the full tensor A. Specifically, we may set $\sigma = \sigma' = \uparrow$, which we assume from now on. Furthermore, spin conservation then implies that $s = s'$. Therefore we abbreviate our full A, p and h tensors to,

$$A^{\uparrow\uparrow}_{\substack{s,s \\ \alpha,\beta}} \to A^{s\alpha\beta} = p^{s\alpha\beta} - h^{s\alpha\beta} \, . \qquad (\text{S-28})$$

Likewise we abbreviate,

$$\mathbb{M}^{\sigma\sigma'}_{\substack{s,s' \\ \alpha,\beta}}(\pm) \to \mathbb{M}^{s\alpha\beta}_{\pm} \, , \qquad (\text{S-29})$$

as used in the main paper. Thus we may write,

$$p^{s\alpha\beta} = \left(\vec{U}^{N;\uparrow}_{\rm gs}\right)^{\dagger} \mathbb{M}^{s\alpha\beta}_{+} \left(\vec{U}^{N;\uparrow}_{\rm gs}\right) \qquad (\text{S-30})$$

$$h^{s\alpha\beta} = \left(\vec{U}^{N;\uparrow}_{\rm gs}\right)^{\dagger} \mathbb{M}^{s\alpha\beta}_{-} \left(\vec{U}^{N;\uparrow}_{\rm gs}\right) \qquad (\text{S-31})$$

$$\mathbb{M}^{s\alpha\beta}_{\pm} = \left(\mathbb{X}^{N;\uparrow}_{\beta s\pm}\right)^{\dagger} \left[E_{\rm gs}\boldsymbol{I} - \boldsymbol{H}^{N\pm1;\frac{1}{2}\pm s}_\phi\right]^{-1} \left(\mathbb{X}^{N;\uparrow}_{\alpha s\pm}\right) \qquad (\text{S-32})$$

$$\mathbb{X}^{N;\uparrow}_{\alpha s\pm} = \left(\vec{\phi}^{N\pm1,\frac{1}{2}\pm s}\right)^{\dagger} d^{(\dagger)}_{r_\alpha s} \left(\vec{\phi}^{N;\uparrow}\right) \qquad (\text{S-33})$$
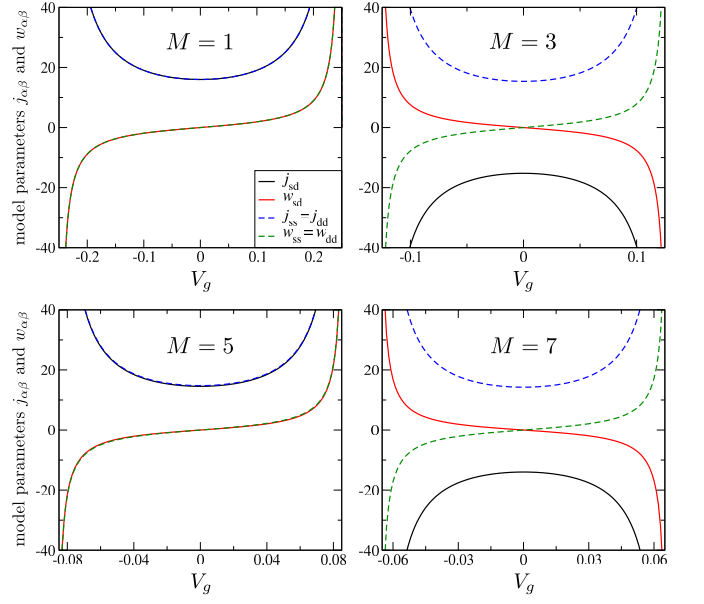

FIG. S-1. Effective model parameters $j_{\alpha\beta}$ and $w_{\alpha\beta}$ as a function of gate voltage V_g from SWT calculations on chains of length $M = 1, 3, 5, 7$ sites, with local interaction U and nearest-neighbour hopping t. In this example we have taken $U/t = 1$ and set $t = 0.5$. Source and drain leads are connected to sites 1 and M. Kondo exchange interactions j_{ss} and j_{dd} (blue dashed lines) are equal and antiferromagnetic throughout the entire gate voltage range shown where the many-body molecule ground state is a spin-doublet. Potential scatterings w_{ss}, w_{dd}, and w_{sd} vanish at the particle-hole symmetric point $V_g = 0$ in all cases. The sign of j_{sd} is seen to alternate, being antiferromagnetic for $M = 4m + 1$ and ferromagnetic for $M = 4m + 3$.

B. SWT results for odd Hubbard chains

As a simple application, we consider the SWT and resulting effective 2CK model parameters as a function of gate voltage V_g for chains of M interacting sites with on-site Coulomb repulsion U, connected by nearest-neighbour hoppings t. The Hamiltonian is given by Eq. S-5, and we take $\epsilon = -U/2$ here so that the system possesses exact particle-hole symmetry when $V_g = 0$. Leads are connected to either end of the chain, Eq. S-6. For odd M, the molecule supports a unique spin-doublet ground state for gate voltages around $V_g = 0$ (the Coulomb blockade transitions to $M \pm 1$ electron states depend on U, and t). When the molecule hosts a spin-doublet ground state, the effective 2CK model, Eq. S-17, describes the low-energy behavior.

Fig. S-1 shows the effective 2CK model parameters $j_{\alpha\beta}$ and $w_{\alpha\beta}$ as a function of gate voltage V_g for odd $M = 1, 3, 5, 7$ as derived using the numerical SWT with $U/t = 1$. We note that the prescription developed above allows the calculations to be performed cheaply even for the $M = 7$ chain using exact diagonalization, with the entire gate-voltage sweep obtained in a few minutes on a standard desktop computer.

The $M = 1$ case is equivalent to a two-lead version of the AIM, and is a special limit since both source and drain lead couple to the same molecule orbital ($r_s = r_d = 1$). This is the only 'molecule' to satisfy 'proportionate coupling', which allows us to reduce the system exactly to a single-channel model. This is achieved by canonical transformation of the lead operators from source-drain basis to even-odd basis,

$$c_{e\sigma} = \frac{1}{\tilde{V}}\left(V_s c_{s\sigma} + V_d c_{d\sigma}\right) \ ,$$
$$c_{o\sigma} = \frac{1}{\tilde{V}}\left(V_d c_{s\sigma} - V_s c_{d\sigma}\right) \ , \qquad \text{(S-34)}$$

where $\tilde{V}^2 = V_s^2 + V_d^2$, such that the odd lead is decoupled. This exact decoupling on the level of the bare Hamiltonian is not possible for $M > 1$. For $M = 1$ however, the model reduces to the 1-channel AIM and the usual SWT results then pertain on mapping to an effective 1-channel Kondo (1CK) model involving only the even lead [3]:

$$\hat{H}_{1CK} = \hat{H}^e_{\text{lead}} + J_{ee}\hat{\vec{S}} \cdot \hat{\vec{s}}_{ee} + W_{ee}\sum_\sigma c^\dagger_{e\sigma} c_{e\sigma} \qquad \text{(S-35)}$$

$$J_{ee} = 2\tilde{V}^2\left[\frac{1}{U + \epsilon + V_g} - \frac{1}{\epsilon + V_g}\right] \ , \qquad \text{(S-36)}$$

$$W_{ee} = -\tilde{V}^2\left[\frac{1}{U + \epsilon + V_g} + \frac{1}{\epsilon + V_g}\right] \ . \qquad \text{(S-37)}$$

On inverting the transformation Eq. S-34 and returning to the physical source-drain lead basis, the effective 1-channel Kondo model Eq. S-35 becomes precisely our original generalized 2CK model, Eq. S-17. However, the underlying single-channel description for $M = 1$ implies additional relations between the coupling parameters that are not present in general [5]. For $M = 1$ we have $j_{ss} = j_{dd} = j_{sd} = j_{ds}$ and likewise $w_{ss} = w_{dd} = w_{sd} = w_{ds}$ (where, as before, we have divided out the hybridization dependence $J_{\alpha\beta} = V_\alpha V_\beta j_{\alpha\beta}$ and $W_{\alpha\beta} = V_\alpha V_\beta w_{\alpha\beta}$). The important conclusion is that the source-drain mixing terms j_{sd} and w_{sd} are equal to the local terms when there is an underlying 1CK description. Although the single-channel limit is certainly not generic for multi-orbital nanostructures, j_{sd} and w_{sd} are typically finite: these are the terms that mediate a source-drain current through the molecular junction. By contrast, for the 2CK critical point we require $j_{sd} = w_{sd} = 0$, which corresponds to a conductance node.

Returning now to Fig. S-1, we see that for $M = 1$ the 1CK condition on the couplings is indeed satisfied. However, more interestingly, we find that $j_{ss} = j_{dd} = j_{sd} = j_{ds}$ and $w_{ss} = w_{dd} = w_{sd} = w_{ds}$ very accurately holds (although not exactly) for $M = 5$, suggesting that (perhaps surprisingly) the odd lead combination is almost decoupled in the $M = 5$ case at energies or temperatures $\ll U$ where the SWT effective model is expected to hold. This holds also for $M = 9$ (not shown) and we conjecture is the case for all $M = 4m + 1$ (note however that the range of gate over which the doublet ground state occurs narrows on increasing M). Furthermore, for
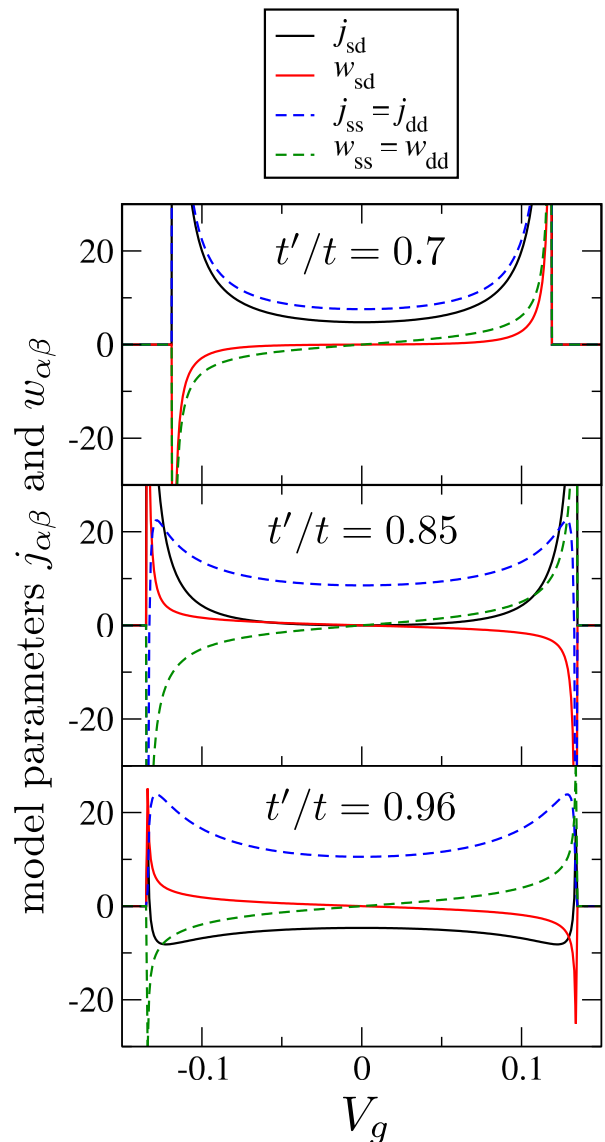

FIG. S-2. Effective model parameters $j_{\alpha\beta}$ and $w_{\alpha\beta}$ as a function of gate voltage V_g from SWT calculations for the $M = 5$ site molecular junction. We take local on-site interaction U and nearest-neighbour hopping t, with $U/t = 1$ and $t = 0.5$ as usual. Here, the next-next-nearest-neighbour hopping t' (connecting sites $1 \leftrightarrow 4$ and sites $2 \leftrightarrow 5$ of the chain) is now also included. The inclusion of t' does not break exact particle-hole symmetry at $V_g = 0$, but does continuously interpolate between $M = 3$ and $M = 5$ limiting cases of the pure chains shown in Fig. S-1 by providing a "shortcut" route through the molecule. This implies the existence of a node in j_{sd} at $V_g = 0$, which we confirm at a critical value of $t' = t'_c \simeq 0.4283$, as shown in the middle panel.

$M = 3$ and $M = 7$ (and again we suspect $M = 4m + 3$ in general), we have $j_{ss} = j_{dd} \simeq -j_{sd} = -j_{ds}$ and $w_{ss} = w_{dd} \simeq -w_{sd} = -w_{ds}$. This also implies an effective 1CK description at low energies or temperatures, but this time involving the *odd* lead combination (and with the even lead decoupling).

C. SWT results for 5-site cluster

The effective 1CK behavior of the odd-length Hubbard chains shown above is particular to the chain geometry around half-filling. Introducing couplings between different sites clearly produces greater complexity on the molecule. Here we consider the 5-site molecular cluster, Eq. S-7, which has sd symmetry, and also an exact ph symmetry at $V_g = 0$.

We expect interesting crossover behavior as a function of the ratio t'/t. For small t'/t, the t' connections are a small perturbation and we expect physics similar to the pure 5-site chain. On the other hand, for large t'/t, we may regard t as the perturbation . Source and drain leads then have a dominant connecting path that is of length 3; the t' bonds offer a kind of 'shortcut' through the $M = 5$ chain. Tuning t'/t therefore allows us to continuously deform between the $M = 5$ and $M = 3$ limits. Since the sign of j_{sd} changes on going from $M = 5$ to $M = 3$ we expect a critical value $t' = t'_c$ where $j_{sd} = 0$ just vanishes at $V_g = 0$. As shown in Fig. S-2, this is precisely what we find. Here we plot the SWT model parameters for the model Eq. S-7, with source and drain leads connected to sites 1 and 5, and for $U/t = 1$ and $t = 0.5$ as a function of gate voltage V_g. The ratio t'/t is increased from top to middle to bottom panels. In the top panel, we see behavior similar to that of the pure $M = 5$ chain shown in Fig. S-1, but with the effective single-channel condition now violated ($j_{ss} = j_{dd} \neq j_{sd}$ and $w_{ss} = w_{dd} \neq w_{sd}$). In the bottom panel we see behavior instead more similar to the pure $M = 3$ chain, with negative j_{sd}. The middle panel shows the 'sweet spot' condition where j_{sd} precisely vanishes at $V_g = 0$ due to many-body QI effects of the competing pathways through the 5-site molecular moiety.

S-III. QI CLASSES

Ref. [4] made a detailed study of many-body QI effects in molecular junctions, focusing on the transport problem within perturbation theory. Alternant hydrocarbon molecules were studied, whose structures can be accommodated on a bipartite graph with no odd loops, and to which the Coulson-Rushbrooke pairing theorem applies [10, 11]. Exchange cotunneling and potential scattering terms equivalent to our J_{sd} and W_{sd} were identified for systems with a net spin-doublet ground state.

A key insight from Ref. [4] is that QI effects in such systems can be classified according to the number of nodes found by varying the gate voltage all the way across a given charge state. In our notation, for a particular molecular junction they define,

$$\mathcal{Q}_W = \frac{\langle \psi_0^{N;\frac{1}{2}}|d_{r_s\uparrow}^{\dagger}|\psi_0^{N-1;0}\rangle\langle\psi_0^{N-1;0}|d_{r_d\uparrow}|\psi_0^{N;\frac{1}{2}}\rangle}{\langle\psi_0^{N;\frac{1}{2}}|d_{r_d\uparrow}|\psi_0^{N+1;1}\rangle\langle\psi_0^{N+1;1}|d_{r_s\uparrow}^{\dagger}|\psi_0^{N;\frac{1}{2}}\rangle} \, , \quad \text{(S-38)}$$

and

$$\mathcal{Q}_J = \frac{\langle \psi_0^{N;-\frac{1}{2}}|d_{r_s\downarrow}^{\dagger}|\psi_0^{N-1;0}\rangle\langle\psi_0^{N-1;0}|d_{r_d\uparrow}|\psi_0^{N;\frac{1}{2}}\rangle}{\langle\psi_0^{N;-\frac{1}{2}}|d_{r_d\uparrow}|\psi_0^{N+1;0}\rangle\langle\psi_0^{N+1;0}|d_{r_s\downarrow}^{\dagger}|\psi_0^{N;\frac{1}{2}}\rangle} \, , \quad \text{(S-39)}$$

where a sum over possible degeneracies of the $N \pm 1$ ground states is implied.

Ref. [4] showed that for bipartite molecules $\mathcal{Q} > 0$ describes the *odd* QI class with an odd number of QI nodes found upon scanning V_g, whereas $\mathcal{Q} < 0$ describes the *even* QI class with an even number of QI nodes. Indeed, $\mathcal{Q}_W > 0$ if the source and drain leads connect to the same sublattice, whereas $\mathcal{Q}_W < 0$ if the source and drain leads connect to different sublattices. Furthermore, bipartite molecules with an odd number of sites (which therefore have a spin-doublet ground state at their ph symmetric point) satisfy the rule $\mathcal{Q}_W = -\mathcal{Q}_J$, meaning that W and J always necessarily belong to different QI classes. In a given molecule charge sector, if W shows an odd number of nodes on scanning V_g then J must show an even number. This is borne out by our SWT results in Fig. S-1, where the odd Hubbard chains (which have leads coupled to the same sublattice) have a single node in W but no nodes in J. Ref. [4] concludes that a true conductance node is therefore 'generally not possible' in such systems since J_{sd} and W_{sd} do not generally have a node at the same V_g.

However, it is also possible that two QI nodes in the even QI class can occur at the same gate voltage (degenerate case). This is precisely what we see in Fig. S-2. W is in the odd QI class with a node in W_{sd} at $V_g = 0$. On the other hand J is in the even QI class and has no nodes for $t' < t'_c$ but two nodes for $t' > t_c$. The two nodes coalesce and are exactly degenerate at $V_g = 0$ when precisely at $t' = t'_c$. This is our 2CK critical point. The QI classification therefore provides a topological perspective on the 2CK phase transition in terms of coalescing and annihilating QI nodes in the 2CK model parameters.

Finally, we note that this analysis holds only for bipartite molecules. Therefore more general structures with odd loops (such as the one considered in Fig. 5 of the main text) need not be so constrained.

S-IV. NUMERICAL RENORMALIZATION GROUP

As noted above, the SWT is a perturbative technique and more sophisticated methods are required to perform the exact mapping [6]. In particular, the SWT does not take into account renormalization effects from the conduction electrons in the leads [8]. It is also confined to the perturbative regime of large U/V. And of course, the *solution* of the effective model is still required to understand the low-energy physics of the system and compute physical observables of interest relevant to experiments, such as the series conductance.

The numerical renormalization group [9] (NRG) is considered the gold-standard method of choice for solving generalized quantum impurity problems, such as those describing the low-energy physics of molecular junctions [5]. Furthermore, experimentally-relevant transport signatures can be accurately calculated using NRG down to low temperatures [12], including renormalization effects from strong electron correlations, such as Coulomb blockade, Kondo effect, and many-body quantum interference phenomena. NRG is a numerically-exact, non-perturbative technique for solving quantum impurity type problems. The NRG method involves the following steps [9].

(i) The source and drain lead density of states $\rho(\omega)$ is divided up into intervals on a logarithmic grid according to the discretization points $\pm D\Lambda^{-n}$, where D is the bare conduction electron bandwidth, $\Lambda > 1$ is the NRG discretization parameter, and $n = 0, 1, 2, 3, ...$. The continuous electronic density in each interval is replaced by a single pole at the average position with the same total weight, yielding $\rho^{\text{disc}}(\omega)$. In this work, as is conventional, we assume metallic leads with a constant density of states $\rho_0 = 1/2D$ within a flat band of half-width D.

(ii) The conduction electron part of the Hamiltonian H_{leads} is then mapped onto semi-infinite tight-binding chains for each lead $\alpha = s, d$:

$$H_{\text{leads}} \to H_{\text{leads}}^{\text{disc}} = \sum_{\alpha,\sigma} \sum_{n=0}^{\infty} t_n \left(f_{\alpha n,\sigma}^\dagger f_{\alpha n+1,\sigma} + \text{H.c.} \right) ,$$

where the Wilson chain coefficients $\{t_n\}$ are determined such that the density of states at the end of each chain reproduces exactly the discretized lead density of states, that is $-\frac{1}{\pi}\text{Im} \langle\langle f_{\alpha 0,\sigma}; f_{\alpha 0,\sigma}^\dagger \rangle\rangle = \rho^{\text{disc}}(\omega)$. Due to the logarithmic discretization, the Wilson chain parameters decay roughly exponentially down the chain, $t_n \sim \Lambda^{-n/2}$. However the detailed form of the t_n encode the specific lead density of states [9].

(iii) The hybridizing molecule orbitals are coupled to site $n = 0$ of the two Wilson chains. We define a sequence of Hamiltonians H_N comprising the molecule and the first $N + 1$ Wilson chain sites,

$$H_N = H_{\text{mol}} + H_{\text{hyb}} + \sum_{\alpha,\sigma} \sum_{n=0}^{N-1} t_n \left(f_{\alpha n,\sigma}^\dagger f_{\alpha n+1,\sigma} + \text{H.c.} \right) ,$$

We now define the recursion relation,

$$H_{N+1} = H_N + \sum_{\alpha,\sigma} t_N \left(f_{\alpha N,\sigma}^\dagger f_{\alpha N+1,\sigma} + \text{H.c.} \right) ,$$

such that the full (discretized) model is obtained as $H^{\text{disc}} = \lim_{N \to \infty} H_N$.

(iv) Starting from the molecule, the chain is built up successively by adding Wilson chain sites using the recursion, Eq. S-40. At each step N, the intermediate Hamiltonian H_N is diagonalized, and only the lowest N_s states are retained to construct the Hamiltonian H_{N+1} at the next step, with the higher energy states being discarded. With each iteration we therefore focus on progressively lower energy scales. Furthermore, the iterative diagonalization and truncation procedure can be viewed as an RG transformation [9], $H_{N+1} = \mathcal{R}[H_N]$.

(v) The sequence of H_N can be viewed as coarse-grained versions of the full model, which faithfully capture the physics at progressively lower and lower temperatures. Useful information is therefore extracted from each step, and physical observables can be obtained at essentially any temperature or energy scale [9].

In this work we use a discretization parameter $\Lambda = 3$ and retain $N_s = 5000$ states at each NRG step. Total charge and spin projection abelian quantum numbers are exploited in the block diagonalization procedure.

In the main text we present results for the linear response series differential conductance $G_c = dI_{sd}/dV_b$ through the molecular junction due to a small source-drain bias voltage V_b. Since anything more complex than the $M = 1$ single-impurity limit does not satisfy the proportionate coupling condition, transport coefficients cannot be simply related to molecule Green's functions. However, the Kubo formula can still be used [13]. Here we use the 'improved Kubo' formulation given in Ref. [12], which produces much more accurate results in the context of NRG calculations for the linear response electrical conductance.

S-V.   2CK CRITICAL POINT

By tuning the ratio t'/t in our 5-site molecular moiety Eq. S-7, the SWT results indicate that we can simultaneously eliminate both j_{sd} and w_{sd} terms of the effective 2CK model. The sd symmetry of the model means that the local Kondo couplings $j_{ss} = j_{dd}$ are equal. Since they are also antiferromagnetic, we expect to be able to realize the QI-2CK effect in this prototype molecular junction. In Fig. S-3 we demonstrate that this is indeed the case, using full NRG results. Furthermore, the QI-2CK effect is found to be remarkably robust, holding beyond the perturbative regime of applicability of the SWT.

In Fig. S-3 we plot the molecule contribution to the total entropy $S_{\text{mol}}(T)$ as a function of temperature T for systems tuned precisely to the QI-2CK critical point ($V_g = 0$ and $t' = t'_c$). Panels (a,b,c) show different interaction strengths U/t (with $t = 0.5$ and $D = 1$ fixed), over a very wide range from perturbative ($U/t = 0.1$) to intermediate/non-perturbative strength ($U/t = 1$), to strong coupling ($U/t = 10$). We have also tested other ratios of U/t and find equivalent results. The different lines plotted in each panel are for different molecule-lead hybridization strengths V. Small V and large U corresponds to the regime of applicability of the SWT calculation, but NRG allows to interrogate the non-perturbative regimes as well – as shown in the figure. In particular, the magenta line in each panel is for a comparatively
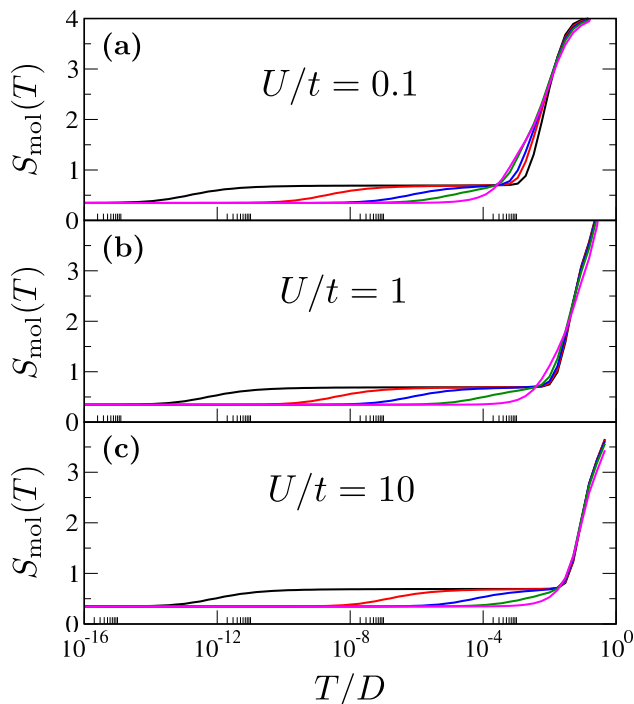
FIG. S-3. NRG results for the molecule contribution to the entropy S_{mol} as a function of temperature T for the 5-site system tuned to the critical point at $t' = t'_c$, for different interaction strengths U/t in panels (a), (b), and (c). As usual we set $t = 0.5$ and the conduction electron bandwidth is $D = 1$. In each case, the molecule-lead hybridization V is varied, showing that the many-body QI-driven 2CK critical point with finite residual ($T = 0$) entropy $S_{\mathrm{mol}} = \frac{1}{2}\ln(2)$ can be realized in all cases. The 2CK Kondo temperature T_{K} is seen to depend sensitively on V (see Fig. 2 of the main paper); but we note that a remarkably large $T_{\mathrm{K}} \sim 10^{-2}U$ can be achieved in all cases, where no incipient local moment regime is observed and RG flow proceeds directly to the 2CK fixed point. For the black, red, blue, green and magenta lines we have $V = 0.03, 0.04, 0.05, 0.06, 0.08$ for $U/t = 0.1$ in panel (a); $V = 0.1, 0.125, 0.15, 0.2, 0.3$ for $U/t = 1$ in panel (b); and $V = 0.3, 0.4, 0.5, 0.6, 0.75$ for $U/t = 10$ in panel (c). The magenta lines show the maximum possible T_{K} achievable for each ratio of U/t.

large V which yields the largest 2CK Kondo temperature T_{K}, while the black lines are for smaller V where the corresponding T_{K} is then smaller.

Interestingly, we find that for all U/t considered, we can access the QI-2CK effect for any V. The hallmark of the 2CK effect is the residual ($T = 0$) molecule entropy of $\frac{1}{2}\ln(2)$ [14], which we here see in all cases. For smaller V the Kondo scale T_{K} is small and we have a window over which the molecule entropy is $\ln(2)$. This corresponds to the local moment regime where the molecule hosts an essentially free spin-doublet state (this is the ground molecule doublet state that we project onto using the SWT). However, the most remarkable observation from our NRG results is that large T_{K} can be realized by tuning V. The largest T_{K} possible for each U/t is in
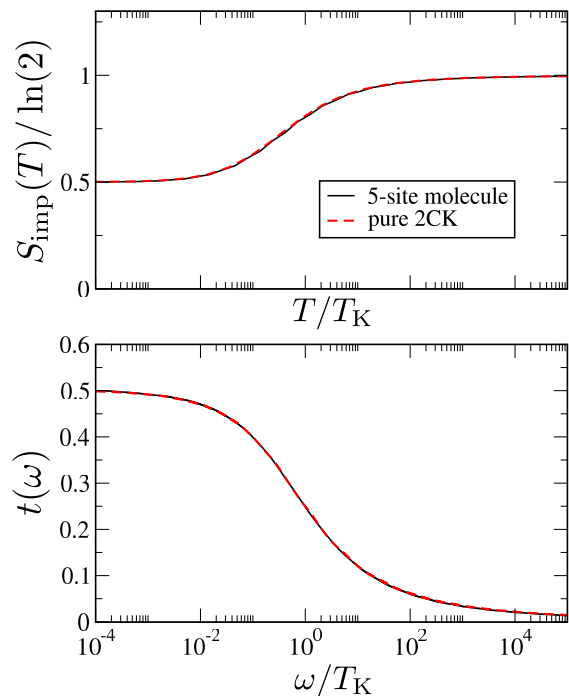
FIG. S-4. To confirm that the many-body QI-driven critical point in the 5-site molecular junction indeed realizes the classic 2CK critical point of the pure 2CK model, we show the 'impurity' entropy $S_{\mathrm{imp}}(T)$ vs T/T_{K} (top panel) and the $T = 0$ scattering t-matrix $t(\omega)$ vs ω/T_{K} (bottom panel) rescaled in terms of the Kondo temperature T_{K} in the universal regime where T_{K} itself is $\ll U, D, t$. Full NRG results for the molecular junction (black solid lines) are compared with those for the pure 2CK model (dashed red lines), and agree perfectly. Shown for $U/t = 10$, $t = 0.5$, $D = 1$, $V = 0.3$, $V_g = 0$, $t' = t'_c$.

fact of order $10^{-2}U$, which is a high-energy scale when compared with the usual exponentially-small Kondo temperatures [3] found in regular single molecule junctions or semiconductor quantum dot devices. This is promising for experimental realization at accessible temperature scales. Finally, we note that as $U \to 0$, the maximum T_{K} also vanishes, meaning that as the non-interacting limit is approached, the 2CK effect also disappears. For typical interaction strengths in molecules or quantum dots, however, we expect the QI-2CK effect to be accessible at unusually high temperatures.

In Fig. S-4 we confirm the SWT prediction that at the critical point of our 5-site molecule we realize the standard 2CK effect. For this, we select a molecule realization in the universal regime with a small T_{K}. When scaled in terms of T_{K}, physical observables should collapse to a universal curve characteristic of the pure 2CK model. The top panel of Fig. S-4 shows NRG results for the entropy, rescaled in terms of T/T_{K} (black solid line), compared with standard results for the pure 2CK model. In the lower panel we show the energy-resolved conduction electron scattering t-matrix $t(\omega)$ at $T = 0$ vs ω/T_{K} for the molecule, compared with universal results of the
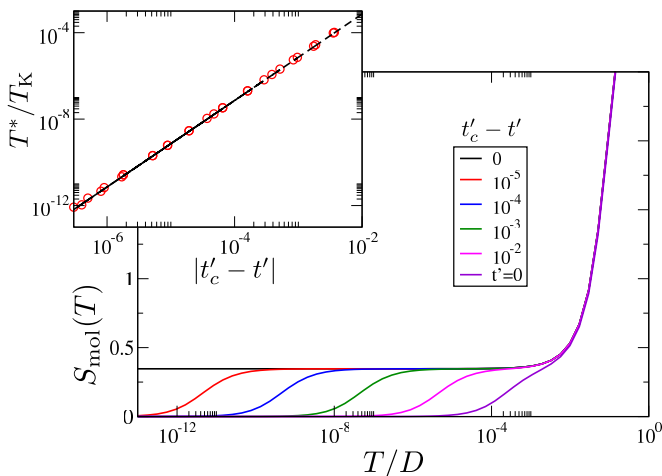
FIG. S-5. NRG results for the Fermi liquid crossover in the 5-site molecular junction near the QI-2CK critical point, with t' successively approaching the critical point at t'_c. Main panel shows the entropy crossover, in which the critical $\frac{1}{2}\ln(2)$ entropy is quenched below T^*. Inset shows the dependence of T^* itself on the perturbation $|t'_c - t'|$. Dashed line fit shows the robust power-law behavior $T^* \sim |t'_c - t'|^2$. We take $U/t = 10$, $V = 0.75$, $t = 0.5$, $D = 1$ and $V_g = 0$.
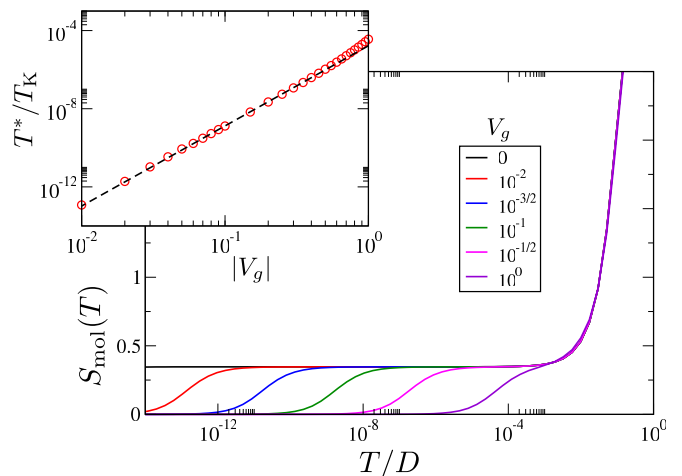
FIG. S-6. NRG results for the Fermi liquid crossover in the 5-site molecular junction, with $t' = t'_c$ but varying the gate voltage V_g to destabilize the QI-driven 2CK critical point. Main panel shows the temperature-dependence of the entropy for each gate voltage setting. Inset shows the resulting crossover scale T^* as a function of V_g, demonstrating with the black dashed line the power-law behavior $T^* \sim |V_g|^4$. We take $U/t = 10$, $V = 0.75$, $t = 0.5$, $D = 1$.

pure 2CK model. Both agree perfectly in the universal regime considered. On the other hand, we note that the standard 2CK model presupposes the existence of an 'impurity' spin-$\frac{1}{2}$ degree of freedom. Our results show that for larger V, the molecule hosts a 2CK critical regime that is not contained within the pure 2CK model since there is no incipient local moment regime.

S-VI. FL CROSSOVER

Having established that the 2CK critical point is accessible in molecular junctions by exploiting the many-body QI effect, we now wish to study in more detail the vicinity of the critical point and the relevant perturbations that drive the system along the NFL-FL crossover towards the stable fully-Kondo-screened ground state. We consider here two perturbations that destabilize the 2CK critical point in our 5-site molecular junction: deviations in the couplings away from $t' = t'_c$ (see Fig. S-5) and deviations in the gate voltage away from particle hole symmetry at $V_g = 0$ (see Fig. S-6).

When the perturbations are sufficiently small, the RG flow for the system proceeds first to the 2CK critical point (with characteristic $\frac{1}{2}\ln(2)$ entropy) on the scale of T_K, and then it flows away from the critical fixed point and towards the FL ground state (with zero entropy) on the emergent low-energy scale T^* [14–16]. For good scale separation $T^* \ll T_K$ we expect a simple power-law dependence of the T^* scale on the strength of the destabilizing perturbation. The power-laws reflect the scaling dimension of the leading RG relevant operators at the fixed

point induced by the perturbation, and are a characteristic fingerprint of the critical fixed point. In the present context of the generalized 2CK model, we expect [14] $T^* \sim aJ_{sd}^2 + bW_{sd}^2$. But J_{sd} and W_{sd} themselves depend on t' and V_g. In Fig. S-5 we show that finite $|t' - t'_c|$ does indeed generate a finite FL scale T^* and corresponding entropy crossover to a fully Kondo screened state. The inset shows specifically that

$$T^* \sim |t' - t'_c|^2 \qquad : \ V_g = 0 \qquad \text{(S-40)}$$

Likewise in In Fig. S-6 we see that the FL crossover is also generated by finite V_g even at $t' = t'_c$ with,

$$T^* \sim |V_g|^4 \qquad : \ t' = t'_c \qquad \text{(S-41)}$$

The difference is because although J_{sd} depends quadratically on both t' and V_g, the critical value of t' is at a finite value t'_c while the critical value of V_g is at $V_g = 0$.

S-VII. ML OPTIMIZATION AND GRADIENT DESCENT

Although we were able to identify conditions for the QI-2CK effect in molecular junctions in the preceding sections using a combination of symmetry arguments and an observation about the SWT for odd chains, a more systematic approach is required for inverse design in general. Indeed, even with the topology of the model Eq. S-7 set, some fine-tuning of the ratio t'/t is still required. On the level of the SWT, one can fix all parameters except t' and then use a simple

root-finding algorithm to determine the value of t' that yields $j_{sd} = 0$. The critical value of t' so determined will however only be an approximation to the true value of t'_c found in full NRG calculations, since the SWT is of course only a perturbative approximation (albeit a rather good one). For the QI-2CK problem, one can again fix all parameters except t' and run the NRG multiple times, varying t', and search for the critical value t'_c that minimizes the FL scale T^*. With only a single parameter to optimize, such a search is very fast and efficient, requiring only a handful of 'function evaluations' to converge exponentially quickly towards the critical point (here 'function evaluation' means either doing the SWT mapping numerically to find j_{sd} or performing an NRG run to determine the T^* scale). Furthermore, the SWT result provides a good starting point guess for the NRG calculation.

However, inverse design of molecular junctions is in general much more complicated than the simplest constrained single-parameter optimization described above. We illustrate this in the main paper with the example of unconstrained optimization of the 4-site molecular cluster, demonstrating that machine learning (ML) methodologies can be applied to the numerical SWT calculation to realize the QI-2CK condition. We envision that this approach will be useful beyond the specific example of the 2CK problem, and will be applicable to the inverse design of molecular junctions for functionalities such as switching, rectification, thermoelectric properties etc, where the desired low-energy effective model parameters are known, but the optimal parent microscopic systems to realize them have yet to be identified.

A. Inverse design using SWT

For molecular junctions, we imagine fixing the lead and hybridization Hamiltonians, and searching through the large configuration space of molecular structures that yield the desired effective model parameters from the SWT. For demonstration here we do not yet consider realistic molecules whose structure and chemistry are determined from *ab initio* methods or from experimental analysis, but rather simply take the parameters of our generalized $\hat{H}_{\mathrm{mol}}$ molecular model to be freely tunable. Consider an abstract model for the isolated molecule of the form,

$$\hat{H}_{\mathrm{mol}} = \sum_i \theta_i \hat{h}_i \qquad (S\text{-}42)$$

with coupling constants θ_i (which we assemble into a vector $\vec{\theta}$) and operators $\hat{h}_i$ that are defined on the molecule Hilbert space. Provided that the molecule ground state over the range of gate voltages of interest is a unique spin-double state, we can apply the numerical SWT prescription described above in Sec. S-II. The desired effective

model parameters are obtained by evaluating Eqs. S-18-S-20 and S-25-S-27.

The desired functionality of the molecular junction places conditions on the effective model parameters $j_{\alpha\beta}$ and $w_{\alpha\beta}$. We encode these into a loss function $\mathcal{L}(\vec{\theta}) = f(j_{ss}, j_{dd}, j_{sd}, w_{ss}, w_{dd}, w_{sd})$ where f is some objective function to be minimized that defines the optimization landscape, whereas $j_{\alpha\beta}$, $w_{\alpha\beta}$ depend implicitly on $\vec{\theta}$ through the SWT calculation. Despite the typically high complexity of $\hat{H}_{\mathrm{mol}}$, the ML optimization of the molecule can be done efficiently by gradient descent (GD). This involves calculating the derivative of the loss function $\vec{\nabla}_\theta \mathcal{L}$ with respect to the optimization parameters $\vec{\theta}$ and taking a finite step in the direction of the gradient vector from an initial guess $\vec{\theta}_0$ to a new guess $\vec{\theta}_1$ such that $\mathcal{L}(\vec{\theta}_1) < \mathcal{L}(\vec{\theta}_0)$. This is repeated iteratively until convergence within some tolerance to the minimum in $\mathcal{L}$, whence we have obtained the optimal set of coupling constants $\vec{\theta}$. We note however that care must be taken since the optimization landscape may contain many local minima or indeed degenerate global minima.

To make this more concrete, consider the generalized 4-site molecule model, Eq. S-8, with $U_m \equiv U = 1$. We will treat the set of single-particle coupling constants t_{mn} and the overall gate voltage V_g as free tuning parameters that comprise the vector $\vec{\theta}$ to be optimized. Focusing on the QI-2CK effect, we demand a spin-doublet ground state giving an effective model for which $j_{sd} = 0$ and $w_{sd} = 0$, as well as $j_{ss} = j_{dd} > 0$. A simple starting point for the loss function is,

$$\mathcal{L}(\vec{\theta}) = a(j_{sd})^2 + b(w_{sd})^2 + c(j_{ss} - j_{dd})^2 + d\sum_\alpha (|j_{\alpha\alpha}| - j_{\alpha\alpha}) \qquad (S\text{-}43)$$

where a, b, c, d are optimization hyperparameters that affect the optimization landscape and hence the learning curve. We also add a term that punishes gate voltages close to the Coulomb blockade steps, since the SWT breaks down in these regimes and the effective parameters $j_{\alpha\beta}$ and $w_{\alpha\beta}$ spuriously diverge. In practice, in a given iteration of the optimization procedure we fix a set of t_{mn} and scan over the entire gate voltage range to identify regions with a spin-doublet ground state, and find the minimum of $\mathcal{L}$ for that gate sweep. Designing a good loss function is the art behind any complex optimization procedure.

In order to perform the GD, we would like the analytic gradient of the loss function. A numerical evaluation is costly when the number of parameters to be optimized is large, and finite-difference methods are inaccurate in practice. Although the analytic gradient with respect to the effective model parameters $j_{\alpha\beta}$ and $w_{\alpha\beta}$ is trivial, the desired gradient with respect to the *bare* model parameters $\vec{\theta}$ is much more challenging. The key step is to work out the derivative of the particle and hole tunneling amplitudes in Eqs. S-25, S-26 with respect to a given tuning parameter θ_i.

An important implication of our SWT formulation is

that the only non-trivial information needed to compute the gradient of the loss function analytically is the derivative of the ground eigenstate $\partial_{\theta_i}\vec{U}_{\text{gs}}$ and the derivative of the ground state energy $\partial_{\theta_i}E_{\text{gs}}$. Suppressing indices to simplify the notation in the following, from Eq. S-25,

$$
\begin{aligned}
\partial_{\theta_i}p = & \left(\partial_{\theta_i}\vec{U}_{\text{gs}}\right)^{\dagger}\mathbb{M}_{+}\vec{U}_{\text{gs}} + \vec{U}_{\text{gs}}^{\dagger}\mathbb{M}_{+}\left(\partial_{\theta_i}\vec{U}_{\text{gs}}\right) \\
& + \vec{U}_{\text{gs}}^{\dagger}\left(\partial_{\theta_i}\mathbb{M}_{+}\right)\vec{U}_{\text{gs}}
\end{aligned}
\tag{S-44}
$$

and similarly for $\partial_{\theta_i}h$. Then from Eq. S-27 it follows,

$$
\begin{aligned}
\partial_{\theta_i}\mathbb{M}_{\pm} = & \\
\mathbb{X}_{\pm}^{\dagger}\left[E_{\text{gs}}\boldsymbol{I} - \boldsymbol{H}_{\phi}\right]^{-1} & \left[\boldsymbol{h}_{\phi}^{i} - \partial_{\theta_i}E_{\text{gs}}\boldsymbol{I}\right]\left[E_{\text{gs}}\boldsymbol{I} - \boldsymbol{H}_{\phi}\right]^{-1}\mathbb{X}_{\pm}
\end{aligned}
\tag{S-45}
$$

where $\boldsymbol{h}_{\phi}^{i} = \vec{\phi}^{\dagger}\hat{h}_i\,\vec{\phi}$ such that $\boldsymbol{H}_{\phi} = \sum_i \theta_i\boldsymbol{h}_{\phi}^{i}$. Note that $\mathbb{X}_{\pm}$, $\boldsymbol{H}_{\phi}$ and $\boldsymbol{h}_{\phi}^{i}$ are all evaluated in the *product* basis and are therefore independent of the optimization procedure. Only $\partial_{\theta_i}\vec{U}_{\text{gs}}$ and $\partial_{\theta_i}E_{\text{gs}}$ must be recomputed at each new optimization step. For the latter, we may simply use the Hellmann–Feynman theorem,

$$
\partial_{\theta_i}E_{\text{gs}} = \langle\psi_{\text{gs}}|\hat{h}_i|\psi_{\text{gs}}\rangle \, ,
\tag{S-46}
$$

whereas the former follows from a standard result in non-degenerate perturbation theory [17],

$$
\partial_{\theta_i}\vec{U}_{\text{gs}} = \vec{\phi}_{\text{gs}}^{\dagger}\sum_{j\neq\text{gs}}\frac{\langle\psi_j|\hat{h}_i|\psi_{\text{gs}}\rangle}{E_{\text{gs}} - E_j}|\psi_j\rangle \, ,
\tag{S-47}
$$

where the sum runs over states in the ground quantum number subspace (N,σ) of the isolated molecule only.

These expressions allow us to compute accurately and cheaply the analytic gradient of the effective model parameters from the SWT, and hence the analytic gradient of any optimization loss function that depends on them. In turn, we may perform GD optimization of our effective model efficiently.

In the main text we demonstrate this with the example of a 4-site molecular cluster given by Eq. S-8 using the loss function Eq. S-43. Starting from a random guess for the parameters $\vec{\theta}_0$, we rapidly converge to a solution satisfying the QI-2CK conditions, as shown in Fig. 5 of the main paper. The parameters used in Fig. 5 resulting from our optimization procedure are $t_{11} \simeq 0.697$, $t_{22} \simeq 0.642$, $t_{33} \simeq 0.480$, $t_{44} \simeq 0.253$, $V_g = 0.42$, $t_{12} \simeq 0.102$, $t_{13} \simeq 0.053$, $t_{14} \simeq 0.1$, $t_{23} \simeq 0.109$, $t_{24} \simeq 0.046$, $t_{34} \simeq 0.169$.

B. Inverse design using NRG

A more sophisticated treatment is provided using NRG which is a non-perturbative method [9], and does not rely on the faithful derivation of a low-energy effective model [6], but can work directly with the bare model (at least for modest molecular complexity [5]). Inverse design of molecular junctions using NRG affords the possibility of engineering loss functions for the optimization that work directly with the physical observables of interest.

For example, in the present case of the QI-2CK effect, the quantum critical point is associated with a vanishing T^* scale. This scale can be read off from the temperature dependence of the entropy, as shown in the main paper and in Figs. S-5, S-6. Defining T^* through the relation $S_{\text{mol}}(T = T^*) = \ln(2)/4$ and a loss function $\mathcal{L}(\vec{\theta}) = T^*$ allows us to use ML methodologies to optimize the model parameters $\vec{\theta}$ to minimize T^* by calculation of the molecule entropy. This is the approach we adopt in this work to find the critical value of t' in the 5-site system. However, alternative approaches can be used. Fig. 4 of the main paper shows that the QI-2CK critical point is also associated with a conductance node at $T = 0$. Therefore an alternative loss function might be $\mathcal{L}(\vec{\theta}) = G_c(T = 0)$.

A numerical (finite-difference) approximation to the gradient of the chosen loss function can be computed by running several standard NRG runs. NRG can then be integrated within a standard GD routine for inverse design model optimization. For constrained models with only a few optimization parameters, this might be sufficient.

However, for more complex problems (especially those for which each NRG run is computationally expensive and optimization efficiency is thus a priority), it is clearly advantageous to have the analytic gradient of the loss function from the NRG calculation. This is more challenging than for the SWT calculation because the NRG algorithm itself is much more complex. Also the loss function might comprise physical observables rather than simply effective model parameters. Fortunately this problem has been overcome recently by using *differentiable programming* techniques [18] with the NRG method. This 'automatic differentiable NRG' method allows exact gradients of NRG observables to be calculated quickly and efficiently [19]. This brings inverse design of molecular junctions using an NRG solver within reach.

S-VIII. NON-INTERACTING LIMIT

To better understand the QI-2CK critical point of the 5-site molecular junction studied above, here we consider the non-interacting $U \to 0$ limit of the model,

$$
\begin{aligned}
H_{\text{mol}} = & t\sum_{\sigma}\left(d_{1\sigma}^{\dagger}d_{2\sigma} + d_{2\sigma}^{\dagger}d_{3\sigma} + d_{3\sigma}^{\dagger}d_{4\sigma} + d_{4\sigma}^{\dagger}d_{5\sigma} + \text{H.c.}\right) \\
& + t'\sum_{\sigma}\left(d_{1\sigma}^{\dagger}d_{4\sigma} + d_{2\sigma}^{\dagger}d_{5\sigma} + \text{H.c.}\right) \\
H_{\text{hyb}} = & V\sum_{\sigma}\left(c_{s\sigma}^{\dagger}d_{1\sigma} + c_{d\sigma}^{\dagger}d_{5\sigma} + \text{H.c.}\right)
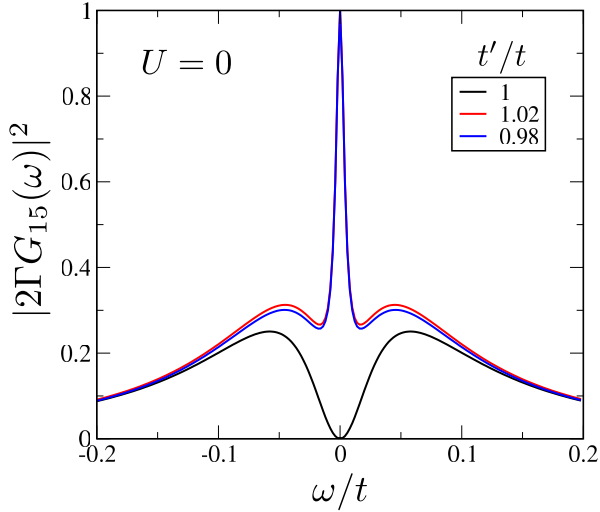\end{aligned}
\tag{S-48}
$$

FIG. S-7. Through-molecule Green's function $G_{15}(\omega)$ for the 5-site molecular junction in the non-interacting ($U = 0$) limit, plotted for $t = 1$ and $\Gamma_s = \Gamma_d = 0.1$ for different t'. From Eq. S-54 the zero-temperature series conductance $G_c(0) = 2e^2/h$ is seen to take the maximum value for a single electron transistor for any $t' \neq t$, but precisely vanishes due to a single-particle QI node at $t' = t$.

which possesses sd-symmetry and particle-hole symmetry. Since $U = 0$ the $\sigma = \uparrow$ and $\downarrow$ sectors are completely independent and can be treated separately. The two sectors are identical due to $SU(2)$ spin symmetry. Here we focus on the $\sigma = \uparrow$ sector for concreteness.

The first question is: what is the analogue of the QI-2CK critical point when $U = 0$? The answer is provided by the SWT calculations shown in Fig. 2 of the main paper. For small but finite U/t we see that the critical value of t' tends to the value of t. This is supported by full NRG calculations. Thus, we deduce that $t'/t \to 1$ as $U/t \to 0$. Below, we therefore examine Eq. S-48 in the vicinity of the point $t'/t = 1$. Indeed, we find that $t'/t = 1$ is a special point.

We start by performing a rotation to an even/odd orbital basis, viz:

$$d_{1^e_o\sigma} = \frac{1}{\sqrt{2}}[d_{1\sigma} \pm d_{5\sigma}] \qquad (S\text{-}49)$$

$$d_{2^e_o\sigma} = \frac{1}{\sqrt{2}}[d_{2\sigma} \pm d_{4\sigma}] \qquad (S\text{-}50)$$

$$c_{e_o\sigma} = \frac{1}{\sqrt{2}}[c_{s\sigma} \pm c_{d\sigma}] . \qquad (S\text{-}51)$$

In this basis, the model exactly decouples into even and odd sectors,

$$H_{\text{mol}} = \sum_{\sigma} \left[(t + t')d_{1e\sigma}^{\dagger}d_{2e\sigma} + \sqrt{2}td_{2e\sigma}^{\dagger}d_{3\sigma} + \text{H.c.} \right]$$

$$+ (t - t') \sum_{\sigma} \left[d_{1o\sigma}^{\dagger}d_{2o\sigma} + \text{H.c.} \right]$$

$$H_{\text{hyb}} = V \sum_{\sigma} \left(c_{e\sigma}^{\dagger}d_{1e\sigma} + c_{o\sigma}^{\dagger}d_{1o\sigma} + \text{H.c.} \right)$$

$$(S\text{-}52)$$

Importantly, we see that the orbital $d_{2o\sigma}$ exactly decouples from the rest of the system when $t' = t$, and sits at zero energy. This directly implies that the $T = 0$ contribution from the molecule to the total entropy of the system is $S_{\text{mol}}(0) = \ln(4)$ at this special point, since all other molecule degrees of freedom are screened by the leads.

By contrast, we know from our NRG results at small but finite U/t where the critical point arises at $t' \simeq t$ that the $T = 0$ residual molecule entropy is $\frac{1}{2}\ln(2)$. The critical point is therefore a genuine non-Fermi liquid (NFL) in the sense that it is not adiabatically connected to the non-interacting limit. However, the energy scale T_K corresponding to the formation of the NFL state also vanishes as $U/t \to 0$ as argued above. We speculate that it is the decoupled single-particle state $d_{2o\sigma}$ of the non-interacting molecule that seeds the NFL state when interactions are turned on.

Finally, we consider dynamical properties of the $U = 0$ molecule. The molecule Green's functions of the lead-coupled system can be simply determined,

$$\boldsymbol{G}_{\text{mol}}^{U=0}(\omega) = \begin{bmatrix} \omega^+ + i\Gamma & -t & 0 & -t' & 0 \\ -t & \omega^+ & -t & 0 & -t' \\ 0 & -t & \omega^+ & -t & 0 \\ -t' & 0 & -t & \omega^+ & -t \\ 0 & -t' & 0 & -t & \omega^+ + i\Gamma \end{bmatrix}^{-1}$$

$$(S\text{-}53)$$

where $[\boldsymbol{G}_{\text{mol}}]_{ij} = \langle\langle d_{i\sigma}; d_{j\sigma}^{\dagger}\rangle\rangle$, $\omega^+ = \omega + i0^+$ and $\Gamma = \pi V^2\rho_0$, with ρ_0 the lead density of states (we have assumed the wide-flat-band limit for simplicity).

Of particular interest is the through-molecule Green's function that connects the source and drain leads, $G_{15}(\omega)$, since this controls series transport in the non-interacting limit via the Landauer formula [12, 20],

$$G_c(T) = \left(\frac{2e^2}{h} \right) \int d\omega \frac{-\partial f(\omega)}{\partial \omega} \times |2\Gamma G_{15}(\omega)|^2 , \quad (S\text{-}54)$$

where $G_c(T)$ is the series electrical conductance dI_{sd}/dV_b resulting when a current I_{sd} flows due to a bias voltage V_b between source and drain leads in linear response, and $f(\omega) = 1/[1 + \exp(\omega/T)]$ is the equilibrium fermi function. The $T = 0$ conductance then follows as $G_c(0) = (2e^2/h) \times |2\Gamma G_{15}(0)|^2$ and depends on the fermi level behavior of the through-molecule Green's function $G_{15}(0)$. Analysis of Eq. S-53 shows that,

$$2\Gamma G_{15}^{U=0}(\omega \to 0) = \begin{cases} -i & : t' \neq t \\ 0 & : t' = t \end{cases} \qquad (S\text{-}55)$$

The full energy-dependence is shown in Fig. S-7, and establishes that for $t' \neq t$ a narrow peak pinned at the fermi energy to $|2\Gamma G_{15}(0)|^2 = 1$ collapses at $t' = t$. Thus the $T = 0$ conductance $G_c(0) = 2e^2/h$ for any $t' \neq t$ but has an exact conductance node $G_c(0) = 0$ for $t' = t$. This is a result of the single-particle QI in the system at $t' = t$, giving rise to destructively interfering paths

through the molecule. We note that in the interacting case $U > 0$ the $T = 0$ conductance also saturates to its maximum $G_c(0) = 2e^2/h$ away from the QI-2CK critical point $t' \neq t'_c$, but series conductance vanishes $G_c(0) = 0$ at the critical point $t' = t'_c$. However, in this case the conductance node is a true many-body QI effect.

[1] L. Lafferentz, F. Ample, H. Yu, S. Hecht, C. Joachim, and L. Grill, Conductance of a single conjugated polymer as a continuous function of its length, Science **323**, 1193 (2009).

[2] J. R. Schrieffer and P. A. Wolff, Relation between the anderson and kondo hamiltonians, Physical Review **149**, 491 (1966).

[3] A. Hewson, *The Kondo Problem to Heavy Fermions* (Cambridge University Press, Cambridge, England, 1993).

[4] K. G. Pedersen, M. Strange, M. Leijnse, P. Hedegård, G. C. Solomon, and J. Paaske, Quantum interference in off-resonant transport through single molecules, Physical Review B **90**, 125413 (2014).

[5] A. K. Mitchell, K. G. Pedersen, P. Hedegård, and J. Paaske, Kondo blockade due to quantum interference in single-molecule junctions, Nature communications **8**, 1 (2017).

[6] J. B. Rigo and A. K. Mitchell, Machine learning effective models for quantum systems, Physical Review B **101**, 241105 (2020).

[7] R. Chan and M. Gulácsi, The exact schrieffer–wolff transformation, Philosophical Magazine **84**, 1265 (2004).

[8] F. Haldane, Theory of the atomic limit of the anderson model. i. perturbation expansions re-examined, Journal of Physics C: Solid State Physics **11**, 5015 (1978).

[9] R. Bulla, T. A. Costi, and T. Pruschke, Numerical renormalization group method for quantum impurity systems, Reviews of Modern Physics **80**, 395 (2008).

[10] C. Coulson and G. Rushbrooke, Note on the method of molecular orbitals, in *Mathematical Proceedings of the Cambridge Philosophical Society*, Vol. 36 (Cambridge University Press, 1940) pp. 193–200.

[11] Y. Tsuji, E. Estrada, R. Movassagh, and R. Hoffmann, Quantum interference, graphs, walks, and polynomials, Chemical reviews **118**, 4887 (2018).

[12] E. L. Minarelli, J. B. Rigo, and A. K. Mitchell, Linear response quantum transport through interacting multi-orbital nanostructures, arXiv preprint arXiv:2209.01208 (2022).

[13] R. Kubo, Statistical-mechanical theory of irreversible processes. i. general theory and simple applications to magnetic and conduction problems, Journal of the physical society of Japan **12**, 570 (1957).

[14] I. Affleck and A. W. Ludwig, Exact conformal-field-theory results on the multichannel kondo effect: Single-fermion green's function, self-energy, and resistivity, Physical Review B **48**, 7297 (1993).

[15] E. Sela, A. K. Mitchell, and L. Fritz, Exact crossover green function in the two-channel and two-impurity kondo models, Phys. Rev. Lett. **106**, 147202 (2011).

[16] A. K. Mitchell and E. Sela, Universal low-temperature crossover in two-channel kondo models, Phys. Rev. B **85**, 235127 (2012).

[17] R. P. Feynman, Forces in molecules, Physical review **56**, 340 (1939).

[18] M. Bartholomew-Biggs, S. Brown, B. Christianson, and L. Dixon, Automatic differentiation of algorithms, Journal of Computational and Applied Mathematics **124**, 171 (2000).

[19] J. B. Rigo and A. K. Mitchell, Automatic differentiable numerical renormalization group, Physical Review Research **4**, 013227 (2022).

[20] R. Landauer, Spatial variation of currents and fields due to localized scatterers in metallic conduction, IBM Journal of research and development **1**, 223 (1957).